ISTANBUL TECHNICAL UNIVERSITY ★ GRADUATE SCHOOL

ASSESSMENT OF SPATIO-TEMPORAL VARIATIONS IN LAKE SURFACE USING LANDSAT IMAGERIES AND GOOGLE EARTH ENGINE

M.Sc. THESIS

Mohammed M. Y. Albarqouni

Department of Geomatics Engineering

Geomatics Engineering Programme

JUNE 2022

ISTANBUL TECHNICAL UNIVERSITY ★ GRADUATE SCHOOL

ASSESSMENT OF SPATIO-TEMPORAL VARIATIONS IN LAKE SURFACE USING LANDSAT IMAGERIES AND GOOGLE EARTH ENGINE

M.Sc. THESIS

Mohammed M. Y. Albarqouni
(501191628)

Department of Geomatics Engineering

Geomatics Engineering Programme

Thesis Advisor: Assoc. Prof. Dr. Filiz Bektaş Balçık

JUNE 2022

İSTANBUL TEKNİK ÜNİVERSİTESİ ★ LİSANSÜSTÜ EĞİTİM ENSTİTÜSÜ

GÖL YÜZEYİNDEKİ MEKANSAL VE ZAMANSAL DEĞİŞİMLERİN LANDSAT GÖRÜNTÜLERİ VE GOOGLE EARTH ENGINE KULLANILARAK DEĞERLENDİRİLMESİ

YÜKSEK LİSANS TEZİ

Mohammed M. Y. Albarqouni
(501191628)

Geomatik Mühendisliği Anabilim Dalı

Geomatik Mühendisliği Programı

Tez Danışmanı: Doç. Dr. Filiz Bektaş Balçık

HAZİRAN 2022

Mohammed M. Y. Albarqouni, a M.Sc. student of İTU Graduate School student ID 501191628, successfully defended the thesis entitled "ASSESSMENT OF SPATIO-TEMPORAL VARIATIONS IN LAKE SURFACE USING LANDSAT IMAGERIES AND GOOGLE EARTH ENGINE", which he prepared after fulfilling the requirements specified in the associated legislations, before the jury whose signatures are below.

Thesis Advisor :	**Assoc. Prof. Dr. Filiz bektaş BALÇIK** Istanbul Technical University	.....
Jury Members :	**Dr. Adalet DERVIŞOĞLU** Istanbul Technical University	.....
	Prof. Dr. Füsun BALIK ŞANLI Yıldız Technical University	.....

Date of Submission : 03 June 2022
Date of Defense : 17 June 2022

To my mother Sabah,

FOREWORD

I would like to give my warmest thanks my unique advisor, Assoc. Prof. Dr. Filiz Bektaş Balçık for her infinite support and guidance through all the stages of writing my thesis. I will be eternally grateful for the opportunities I have been given. Also, I would like to express my gratitude to Dr. Nur Yağmur for her valuable contribution and assistance to my research.

I would like to express the deepest thanks and appreciation to my parents, my brother, and my sisters, who have supported me since the day I was born. Without their support, I never would have been able to go this far in life.

Finally, I would want to thank God for allowing me to overcome all obstacles; I have seen your direction on a daily, and I will continue to rely on you forever.

June 2022

Mohammed M. Y. Albarqouni

(Civil and Geomatics Engineer)

TABLE OF CONTENTS

Page

FOREWORD ..... **IX**
TABLE OF CONTENTS ..... **XI**
ABBREVIATIONS ..... **XIII**
LIST OF TABLES ..... **XV**
LIST OF FIGURES ..... **XVII**
SUMMARY ..... **XIX**
ÖZET ..... **XXI**
1. INTRODUCTION **1**
1.1 Purpose of The Thesis 2
1.2 Literature Review 3
1.2.1 Remote sensing indices to determine water surface area 4
1.2.1.1 The used of satellite data and remote sensing indices in Türkiye's natural lakes 7
1.2.2 Lake Surface Water Temperature (LSWT) 9
2. REMOTE SENSING **11**
2.1 Remote Sensing of Water Surfaces 11
3. STUDY AREA AND SATELLITE DATASETS **13**
3.1 Study Area 13
3.2 Satellite Data 15
3.2.1 Properties of Landsat TM and OLI/TIRS sensors 15
3.2.2 ERA5-Land and TerraClimate monthly satellite dataset 18
4. METHODOLOGY **19**
4.1 Lake Water Surface Area Calculation Using GEE Platform 21
4.1.1 Selection of image collection used in analyses and apply the cloud filtering 22
4.1.2 Normalized Difference Water Index (NDWI) Calculation 23
4.1.3 Accuracy assessment of NDWI maps 24
4.1.4 Lake water surface area calculations 27

4.2 Displaying Surface Water Area Time Series for each Lake 28
4.3 Lake Surface Water Temperature (LSWT) Calculations 29
4.4 Relationship Between Lake Surface Extent and LSWT Variables 32
5. ANALYSIS AND RESULTS 35
5.1 Accuracy Assessment of Extracted NDWI Maps 35
5.2 Spatio-temporal Changes in Lake Water Extent 36
5.2.1 Lake Burdur 36
5.2.2 Lake Egirdir 40
5.2.3 Lake Beysehir 44
5.3 Relationship Between LSWT and Lake Water Extent Changes 49
5.3.1 LSWT of Lake Burdur 49
5.3.2 LSWT of Lake Egirdir 51
5.3.3 LSWT of Lake Beysehir 53
5.4 Meteorological Parameters and Correlation Analysis with LSWT and Lake Water Extent 55
6. CONCLUSIONS AND RECOMMENDATIONS 61
REFERENCES 65
CURRICULUM VITAE 73

ABBREVIATIONS

API : Application Programming Interface
ASTER : Advanced Spaceborne Thermal Emission and Reflection Radiometer
AVHRR : Advanced Very High-Resolution Radiometer
AWEInsh : Automated Water Extraction Index (for non-shadow)
AWEIsh : Automated Water Extraction Index (for shadow)
BT : Brightness Temperature
EVI : Enhanced Vegetation Index
GB : Gigabyte
GDNCNP : General Directorate of Nature Conservation and National Parks
GEE : Google Earth Engine
GIS : Geographic Information System
IDE : Integrated Development Environment
IFOV : Instantaneous Field of View
LST : Land Surface Temperature
LSWT : Lake Surface Water Temperature
MNDWI : Modified Normalized Difference Water Index
MoAF : Ministry of Agriculture and Forestry
MODIS : Moderate Resolution Imaging Spectroradiometer
MSS : Multispectral Scanner
NDVI : Normalized Difference Vegetation Index
NDWI : Normalized Difference Water Index
NIR : Near-Infrared
OLI : Operational Land Imager
SPOT : Systeme Probatoire d'Observation de la Terre
SWIR : Short-wave Infrared
TIRS : Thermal Infrared Sensor
TM : Thematic Mapper
TOA : Top of Atmospheric
USGS : United States Geological Survey
VIIRS : Visible Infrared Imaging Radiometer Suite Visible Infrared Imaging Radiometer

LIST OF TABLES

Page

Table 3.1 : Various properties of study lakes (URL 4). **15**
Table 3.2 : Spectral and Spatial Resolutions of TM & OLI/TIRS sensors (URL 6). **17**
Table 4.1 : Number of images used for each lake. **20**
Table 4.2 : The confusion matrix (Stehman, 2014)..... **26**
Table 5.1 : The accuracy assessment of extracted water pixels with NDWI. **35**
Table 5.2 : Lakes' maximum and minimum surface water area values as well as their recurrence dates..... **48**
Table 5.3 : The monthly correlation analysis of meteorological parameters with LSWT and water surface area. **59**

LIST OF FIGURES

Page

Figure 2.1 : Spectral characteristics of water, soil, and vegetation (Lillesand et al, 2015). **12**
Figure 3.1 : The Study Area's Location Map, (1) Lake Burdur, (2) Lake Egirdir, and (3) Lake Beysehir. **14**
Figure 3.2 : Visual comparison of Landsat spectral bands (URL 5)..... **16**
Figure 4.1 : The methodology's flowchart. **19**
Figure 4.2 : The number of used satellite images for each year. **21**
Figure 4.3 : A view of the GEE code in conjunction with the Code Editor. **22**
Figure 4.4 : Accuracy assessment using random point selection method for the largest water surface..... **27**
Figure 5.1 : Temporal changes of water surface extent and its trendline for Lake Burdur between 2000 and 2021. ..... **38**
Figure 5.2 : Seasonal water surface extent changes in Lake Burdur. **39**
Figure 5.3 : Spatial changes in water surface area according to years for Lake Burdur. **39**
Figure 5.4 : Long-term annual water surface area variations of Burdur Lake..... **40**
Figure 5.5 : Temporal changes of water surface extent and its trendline for Lake Egirdir between 2000 and 2021. ..... **42**
Figure 5.6 : The seasonal water surface extent changes of Lake Egirdir..... **43**
Figure 5.7 : Spatial changes in water surface area according to years for Lake Egirdir. **43**
Figure 5.8 : Long-term annual water surface area variations of Egirdir Lake..... **44**
Figure 5.9 : Temporal changes of water surface extent and its trendline for Lake Beysehir between 2000 and 2021. ..... **46**
Figure 5.10 : The seasonal water surface extent changes of Lake Beysehir..... **47**
Figure 5.11 : Spatial changes in water surface area according to years for Lake Beysehir. **47**
Figure 5.12 : Long-term annual water surface area variations of Beysehir Lake..... **48**
Figure 5.13 : The long-term annual average LSWT for the three lakes. **49**
Figure 5.14 : The temporal changes in surface extent of Burdur Lake with the LSWT variable..... **50**
Figure 5.15 : The spatial changes of Burdur Lake’s surface area with LSWT for: (a) summer 2000, (b) autumn 2000, (c) summer 2021, and (d) autumn 2021. ..... **51**
Figure 5.16 : The temporal changes in surface extent of Egirdir Lake with the LSWT variable..... **52**

Figure 5.17 : The spatial changes of Egirdir Lake's surface area with LSWT for: (a) summer 2000, (b) autumn 2000, (c) summer 2021, and (d) autumn 2021..... **53**
Figure 5.18 : The temporal changes in surface extent of Beysehir Lake with the LSWT variable. **54**
Figure 5.19 : The spatial changes of Beysehir Lake's surface area with LSWT for: (a) summer 2000, (b) autumn 2000, (c) summer 2021, and (d) autumn 2021. .. **54**
Figure 5.20 : Scatter plot and correlation values between LSWT and MODIS LST for all three lakes. **55**
Figure 5.21 : Long term time series statistics of produced LSWT and temperature dataset of ERA5 and TerraClimate **(a)** Burdur Lake; **(b)** Beysehir Lake and **(c)** Egirdir Lake. 57
Figure 5.22 : Long term time series statistics of (a) precipitation and (b) evapotranspiration of TerraClimate for all lakes..... **57**

ASSESSMENT OF SPATIO-TEMPORAL VARIATIONS IN LAKE SURFACE USING LANDSAT IMAGERIES AND GOOGLE EARTH ENGINE

SUMMARY

The purpose of this research is to determine the lake's water surface area and the Lake Surface Water Temperature (LSWT), as well as to give a long-term analysis of the spatial and temporal relationships between these variables. Lake Burdur, Lake Egirdir, and Lake Beysehir were the three lakes in Türkiye's Lakes Region that were taken into consideration to be used as testing sites.

Lakes are crucial to the ecosystem and ecological stability. For the preservation and development of such sensitive regions, continual monitoring using accurate and dependable sources is required. The development of remote sensing technology provides a significant opportunity for the determination, monitoring, and assessment of the current state of lakes. Specifically, the improvement of satellite images spatial and spectral resolutions contributes to this potential.

Mapping water surface area is essential for agriculture, economic, and the structure and function of the ecosystem, as well as for the extent of lakes' water surfaces. Remote sensing methods were used to comprehend the long-term variations in the water surface area of Lake Burdur, Egirdir, and Beysehir. Google Earth Engine (GEE) is a cloud-based platform that applies operations to Landsat satellite images, was used to perform the analysis.

In the study, two satellite sensors; Landsat 5 TM and Landsat 8 OLI/ TIRS, were employed to cover as much of the research period from 2000 to 2021 as possible. Landsat 8 OLI/TIRS gives coverage from 2013 through 2021, while Landsat 5 TM provides coverage from 2000 to 2011. There was no available satellite data for 2012. Also, ERA5-Land and TerraClimate monthly satellite dataset were used in this study to show whether there is correlation between water surface area and LSWT with meteorological parameters (temperature, evaporation and precipitation).

The first chapter discusses the relevance of lakes to the ecosystem and global climate, as well as the information on water body extraction using satellite images acquired by remote sensing was presented. This chapter also discusses the study's scope and objectives.

The second chapter presents the role of remote sensing and satellite data in extracting and monitoring the spatio-temporal changes of water surfaces.

The third chapter introduces the study area and clarified all of its features, in addition to providing the satellite data utilized in the analysis. Thus, a total of 606 Landsat images were collected and analyzed through GEE cloud platform.

In the fourth chapter, the Normalized Difference Water Index (NDWI) was utilized to extract the water pixels in order to determine the surface water extent from the image inventory. Thus, the procedure of calculating surface water area and LSWT has been explained in detail via the used equations and GEE code. The accuracy assessment for the largest and smallest surface water area for each lake was evaluated using the random point selection method and confusion matrix. Moreover, the water surface area changes of the three lakes and the LSWT variable, as well as their relationship with one to another, were analyzed to clarify the effects of an increase or decrease in LSWT over the extent of the lake's surface water.

In the fifth chapter, the daily, seasonal, and annual variations in each lake surface area across the research period were presented. The findings from the study indicate that by using NDWI, water pixels can be extracted rather accurately, with an overall accuracy of more than 98% for the surface area of all lakes. Between 2000 and 2021, the water surface area value of Lake Burdur decreased significantly by more than 22%, while for Lake Egirdir it has dropped slightly by less than 4%, and for Lake Beysehir has not changed noticeably, it has decreased by roughly less than 1%. After analyzing the LSWT values, it can be established that they increased in all lakes except for Beysehir over the study time period. Thus, Burdur Lake's LSWT increased by more than 2.1°C, Egirdir Lake heightened by more than 0.3°C, and Beysehir Lake decreased by more than 1.4°C. The obtained results were evaluated with meteorological parameters and our findings showed that human-induced activities were more dominant than climate effects over the lakes.

In the sixth chapter, the study's findings were reviewed and discussed.

GÖL YÜZEYİNDEKİ MEKANSAL VE ZAMANSAL DEĞİŞİMLERİN LANDSAT GÖRÜNTÜLERİ VE GOOGLE EARTH ENGINE KULLANILARAK DEĞERLENDİRİLMESİ

ÖZET

Bu araştırmanın amacı, gölün su yüzey alanını ve Göl Yüzey Suyu Sıcaklığını (LSWT) belirlemek ve bu değişkenler arasındaki mekansal ve zamansal ilişkilerin uzun vadeli bir analizini vermektir. Türkiye Göller Bölgesi'nde yer alan üç büyük göl, Burdur Gölü, Eğirdir Gölü ve Beyşehir Gölü, çalışma alanı olarak belirlenmiştir.

Göller ekosistem ve ekolojik döngü için çok önemlidir. Bu tür hassas bölgelerin korunması ve geliştirilmesi için doğru ve güvenilir kaynaklar kullanılarak sürekli izlenmesigerekmektedir. Uzaktan algılama teknolojisinin gelişimi, göllerin mevcut durumunun belirlenmesi, izlenmesi ve değerlendirilmesi için önemli bir fırsat sunmaktadır. Spesifik olarak, uydu görüntülerinin mekansal ve spektral çözünürlüklerinin iyileştirilmesi bu potansiyele katkıda bulunmaktadır.

Su yüzey alanının haritalanması, tarım, ekonomi ve ekosistemin yapısı ve işlevi açısından önem arzetmektedir. Burdur, Eğirdir ve Beyşehir göllerinin su yüzey alanındaki uzun vadeli değişimleri anlamak için uzaktan algılama yöntemleri kullanılmıştır. Su yüzey alanlarının uydu görüntülerinden belirlenmesi için Normalize Edilmiş Fark Su Indisi (Normalized Difference Water Index - NDWI) kullanılmıştır. NDWI ve göl su yüzey sıcaklığı (Lake Water Surface Temperature - LSWT) yöntemleri Google Earth Engine (GEE) ortamında Landsat uydu görüntülerine uygulanmıştır. GEE, uydu görüntüleri üzerinde analizleri gerçekleştirmek ve büyük veri işlemek için kullanılan bulut tabanlı bir platformdur.

Çalışmada 2000'den 2021'e kadar olan çalışma dönemini kapsamak üzere iki uydu verisi; Landsat 5 TM ve Landsat 8 OLI/TIRS, kullanıldı. Landsat 8 OLI/TIRS 2013'ten 2021'e kadar olan zaman aralığını kapsarken, Landsat 5 TM 2000'den 2011'e kadar kapsama sağlar. 2012 yılında ise elverişli uydu görüntüsü bulunamamıştır. Ayrıca tez çalışması kapsamında ERA5-Land ve TerraClimate aylık uydu veri seti kullanılarak su yüzey alanı ve LSWT'nin meteorolojik parametreler (sıcaklık, buharlaşma ve yağış) ile arasında bir ilişki olup olmadığı araştırılmıştır.

Birinci bölümde, göllerin ekosistem ve küresel iklim ile olan ilişkisi tartışıldı ve uzaktan algılama ile elde edilen uydu görüntüleri kullanılarak su kütlesinin çıkarılması hakkında literatürden bilgiler sunuldu. Bu bölümde ayrıca çalışmanın kapsamı ve amaçları tartışılmaktadır.

İkinci bölüm, su yüzeylerinin mekansal-zamansal değişimlerini tespit etme ve izlemede uzaktan algılama ve uydu verilerinin rolü verilmiştir.

Üçüncü bölümde, çalışma alanlarının tüm özellikleri ve öneminin yanı sıra analizde kullanılan uydu verilerinin özellikleri detaylarıyla birlikte verilmiştir.. Hava koşullarından etkilenmesiyle bilinen optik görüntülerdeki bulut probleminden dolayı uydu görüntüleri %10 bulut filtresine tabi tutularak seçilmiştir. Böylece toplamda 606 Landsat görüntüsü seçilerek ve GEE bulut platformu üzerinde analizler gerçekleştirilmiştir.

Dördüncü bölümde, uydu görüntülerinden su yüzey alanını belirlemek için kullanılan ve su piksellerini tespit etmede oldukça başarılı olan NDWI ve su yüzey sıcaklığını tespit etmek için kullanılan LSWT yöntemlerinin metodolojisi açıklanmıştır. Su yüzey alanı ve LSWT hesaplama prosedürü, kullanılan denklemler ve GEE kodu ile ayrıntılı olarak verilmiştir. Her göldeen büyük ve en küçük su yüzey alanı için doğruluk değerlendirmesi, rastgele nokta seçim yöntemi ve hata matrisi değerlendirmesi açıklanmıştır.

Ayrıca, üç gölün su yüzey alanı değişiklikleri ve LSWT ile olan ilişkileri, LSWT'de meydana gelen artışın veya azalmanın gölün su yüzey alanı üzerindeki etkilerini belirlemek için analiz edildi.

Beşinci bölümde, araştırma süresi boyunca her bir göl yüzey alanındaki günlük, mevsimlik ve yıllık değişimler sunulmuştur. Çalışmadan elde edilen bulgular, NDWI kullanılarak su piksellerinin, tüm göllerin yüzey alanı için %98'in üzerinde elde edilen genel doğrulukla, oldukça doğru bir şekilde tespit edilebileceğini göstermektedir. 2000-2021 yılları arasında Burdur Gölü'nün su yüzey alanı değeri %22'in üzerinde önemli bir ölçüde azalırken, Eğirdir Gölü için bu değer yaklaşık olarak %4, Beyşehir Gölü için ise gözle görülür bir değişiklik göstermeyerek % 1 azalmaktadır LSWT değerleri analiz edildikten sonra, çalışma süresi boyunca Beyşehir hariç tüm göllerde arttığı tespit edilebilir. Böylece Burdur Gölü'nün su yüzey sıcaklığı 2.1°C'nin üzerinde artış gösterirken, Eğirdir Gölü‘nde 0.3°C yükselmektedir. Beyşehir Gölü’nde ise yaklaşık olarak 1.4°C azalmıştır. Elde edilen sonuçlar, ERA5-Land ve TerraClimate verilerinden elde edilen meteorolojik parametrelerle değerlendirilmiş ve bulgular göller üzerinde insan kaynaklı faaliyetlerin iklim etkilerinden daha baskın olduğunu göstermiştir.

Altıncı bölümde, çalışmanın bulguları gözden geçirilmiş ve tartışılmıştır.

1. INTRODUCTION

Every country and each nation trying to find a way to preserve water and use the least amount of water as the lives of most of humans depend upon it. Rivers, lakes, oceans, and wetlands, for example, are vital to the environment, ecological balance, and hydrological cycle (Zhang et al, 2016; Dörnhöfer et al, 2016). Lakes are among the most significant water resources. They cover 1.8 % of the world's land area and have an effect on the ecosystems that surround them (Messager et al, 2016). Lakes are crucial to the ecosystem, global climate, and sustainable development because of their several roles, including providing drinking water and regulating climate change, as well as functioning as natural rehabilitation sites, fishing waters, and reservoirs for groundwater. Surface water area distribution is critical for water resource planning and management (Jiang et al, 2014; Ji et al, 2015; Masocha et al, 2018). The ability to determine water bodies is useful in a variety of situations, including lake and watershed definition, flood prediction, and water resource monitoring (Ouma and Tateishi, 2007).

Annual or intra-annual changes in surface water may result from climate change and human activity, which have a significant impact on human civilization and ecosystems (Dai, 2013; Lehner, 2016; Xia et al, 2019). Where the primary causes of inland water body deterioration and loss include land use changes, greatly expanded agriculture, water diversion by dams and canalization, air and water pollution, and nutrient dumping (Ramsar, 2006). Changes in water surface area caused by human activities are related to water withdrawals for agricultural and commercial activities. Spatio-temporal mapping of lake surface water extent is critical for ecological and environmental impact assessment. As a result, decision makers benefit from accurate and reliable data on the dynamics of lake water surfaces while making decisions on how to safeguard them, by enabling them to develop long-term management strategies, and determining the lake's water budget.

Surface water extent changes can be studied more effectively using remote sensing technologies. Remote sensing is more efficient than conventional in situ measurements because it can continually monitor the Earth's surface at a variety of scales.

With the use of satellite images, remote sensing data can be used to map the extent of water bodies and track changes in their dynamics on a regular and frequent basis. These data are both spatially explicit and frequent (Huang et al, 2018).

To reduce uncertainty in mapping results, it is difficult to determine the exact time of year for a single image, thus there is 21 years period of the study. Consequently, comprehensive research is required to explore the ongoing alteration of surface water regions by utilizing sufficient images captured over several seasons and years.

1.1 Purpose of The Thesis

Due to the obvious detrimental implications of both human and climatic change, monitoring surface water extents is considered to be one of the primary study areas in remote sensing. In terms of environmental, ecological, and economic benefits, lakes are considered to be one of the most valuable and important water resources. The specific purpose of this study is to determine the spatio-temporal changes in surface water body areas of Lake Burdur, Egirdir, and Beysehir over the 21-year period from 2000 to 2021, as well as analyze the relationship between the lake water surface area changes and the Lake Surface Water Temperature (LSWT) via Google Earth Engine (GEE) using remote sensing images. Regular and exact measurements of the lake surface area are essential to establish the long-term spatio-temporal changes in surface water area to achieve water resource balance. The following are the study's objectives:

(1) A time series investigation of lake water extent changes was conducted using remote sensing images and the GEE cloud computing platform.
(2) Employing the Normalized Difference Water Index (NDWI) to calculate the surface water areas for each lake and determine its accuracy in extracting water pixels.
(3) Studying the alleged connections between lake water extents and LSWT variable.
(4) Analyzing the correlation analysis of the obtained results with meteorological parameters (i.e., precipitation, temperature and evaporation).

The scope of the study covers the determination of the water surface area and monitoring its spatio-temporal changes during 21-years period. In order to comprehend the long-term changes of the surface water extent, the open surface water was mapped using all available Landsat 5 Thematic Mapper (TM) and Landsat 8

Operational Land Imager (OLI)/Thermal Infrared Sensor (TIRS) images from 2000 to 2021.

Due to the free availability of petabyte scale Landsat data, researchers have been able to utilize all available Landsat images to get better gather surface water change information since 2008 (Wang et al, 2019). Simultaneously, in recent years, a multitude of cloud computing platforms have been developed to analyze large-scale geospatial data without needing a great deal of technical expertise or effort, and they have shown a tremendous amount of value in terms of large-scale land cover mapping.

The GEE is a cloud computing platform that can handle data in an innately parallel, high-performance manner and comprises multi-petabytes of distant sensing data that has been preprocessed to be ready-to-use freely and effectively (Gorelick et al, 2017). This platform supports several large-scale geoscientific projects, including forest cover mapping, surface water mapping, and urban land cover mapping, among others (Hird et al, 2017). Thus, this platform was used in our study to determine the spatio-temporal changes of water extent in the study lakes over a study period (2000–2021).

1.2 Literature Review

Remote sensing has been used as a cost-effective method to monitor the spatial and temporal changes in surface water without direct contact with the objects or the ground (Ozesmi and Bauer, 2002; Asokan and Anitha, 2019). In land use and land cover mapping with different time-space spectra, remote sensing image data are exploited because of their broad coverage, high return frequency, wealth of information, and comparatively inexpensive cost. At a given time, satellite images enable the identification of water bodies over a large region. Since satellite data is readily available and time-efficient, remote sensing technology has become one of the most frequently utilized tools for identifying water bodies in recent years (Zhang et al, 2016; Zhou et al, 2017).

The satellite data which is extensively employed in water surface area mapping and monitoring their dynamic changes, are include the Advanced Very High-Resolution Radiometer (AVHRR) Holben (2007), Moderate Resolution Imaging Spectroradiometer (MODIS) (Li et al. 2013; Feng 2019), Systeme Probatoire d'Observation de la Terre (SPOT) Harvey and Hill (2010), Visible Infrared Imaging

Radiometer Suite Visible Infrared Imaging Radiometer (VIIRS) Li et al. (2018), Landsat (Mueller et al. 2016; Chen et al. 2018; Wang et al. 2020) and Sentinel 1 and 2 (Du et al. 2016; Yang et al. 2017) satellite images. The Landsat satellite series is one of the most used optical sensors in surface water and other environmental studies, with its long-term data record and extensive return coverage, the Landsat satellites such as TM and OLI/TIRS have provided one of the most useful datasets for detecting and monitoring the earth's surface since 1972, which is also a continuous dataset with high temporal precision to the scientific community for free (Feyisa et al, 2014).

1.2.1 Remote sensing indices to determine water surface area

The detection of surface water bodies is critical to remote sensing researches. Several surface water body information extraction techniques (Behera et al. 2012; Du et al. 2012; Rokni et al. 2014; Du et al. 2016; Wang et al. 2020) have been developed because of their cruciality for converting remotely sensed images into data that could be used for applications, such as lake surface water mapping (Li et al, 2013). On the basis of remote sensing data, surface water extraction methods can be divided into two categories: machine learning algorithms and traditional algorithms.

It is difficult to quickly map large regional areas, such as a nation, using machine learning algorithms since sample selection and algorithm training need expert knowledge. Traditional water surface extraction techniques can be classified into two types based on their use of several bands: single-band and multi-band methods, which can be further classified into the inter-spectral relation method and the water index method. Multi-band methods are more preferable than single-band methods for water extraction because they make advantage of the varied reflectivity differences between water and other land cover types. Thus, water indices have been applied effectively to extract surface water using remotely sensed data and provide the advantages of accurate, easy, rapid, and repeatable extraction of surface water data that captures the considerable intra-annual and inter-annual water changes (Xia et al, 2019; Wang et al, 2020).

The water index method is used in conjunction with other remote sensing indices to determine the substantial difference between a water body feature and a non-water body feature, where water extraction is quite precise. At the same time, when

extracting huge amounts of water, this approach has the benefits of speed, precision, simplicity, resilience, and reproducibility (Wang et al, 2020).

Many different remote sensing water indices have been developed and can extract water bodies more accurately, quickly, and easily using the combination of spectral bands in the satellite images. The spectral water index methods are as:

Normalized Difference Vegetation Index (NDVI) uses near-infrared and red wavelengths to quantify vegetation. Near-infrared (NIR) and green light are reflected by vegetation, whereas red and blue light are absorbed. Although the primary purpose of this index is to detect vegetation, it was also effective in identifying water bodies. According to Rokni et al. (2014), NDVI accuracy was 99.06 % in 2000 and 98.91 % in 2010 when comparing different indices in mapping the area of Lake Urmia.

The NDWI was introduced by McFeeters (1996). NDWI is an index that maximizes water reflection in the green band while minimizing water reflectance in the NIR band (Xu, 2007). The NDWI scale ranges from -1 to +1, where NDWI > 0 denotes water, while NDWI ≤ 0 denotes non-water. Li et al. (2013) state that the NDWI, according on the green band and the Shortwave Infrared (SWIR) band of the Advanced Land Imager (ALI) sensor is the very best indicator for determining the surface water mapping of the lake. Also, according to Ceyhan (2016), the best approach for distinguishing wet, moist, and dry classes is NDWI, which was selected as a method to detect and determine the water surface extent for Lake Tuz.

The NDWI is utilized in our study to identify water pixels in the study lakes since many studies (Wendleder et al. 2018; Abujayyab et al. 2021; Dervisoglu 2021; Firatli et al. 2022) showed that it provided satisfactory results. The NDWI is used to extract the water surface and its dynamic changes with high degree of accuracy in the extraction of water pixels (Ali et al, 2019). The threshold value of zero was suggested for extracting surface water from Landsat images, with all positive NDWI values classed as water and all negative NDWI values, including zero, classified as non-water. The NDWI for each satellite applied in this study is computed using the GEE platform.

The Modified Normalized Difference Water Index (*M*NDWI) employs green band and SWIR band, it can extract the water surface body with high accuracy. To address the inseparability of built-up regions, Xu (2007) suggested this index. In research to determine which water index has the highest functioning in extraction at three distinct

study locations in the Yangtze River Basin, Li et al. (2013) discovered that the *M*NDWI is the most effective index for detecting water bodies. Wang et al. (2020) also found that *M*NDWI could significantly increase the improvement of open water features, it can distinguish water from non-water objects rapidly and correctly in the Hetao Plain, China.

The Automated Water Extraction Index (AWEI) uses a single threshold to locate water features in Landsat images time series. It is include two indices; $AWEI_{nsh}$ works well when there are no shadows in the image, while the $AWEI_{sh}$ is a better version of the first one that differentiates water pixels from shadow pixels, as introduced by Feyisa et al. (2014). Based on Rokni et al. (2014) research, AWEI was employed for the extraction of Lake Urmia surface area from Landsat imagery data, and the index shows an overall accuracy of 96.63%t in 2000 and 94.06 % in 2010.

According to Bai et al. (2011), multi-temporal Landsat data was utilized to determine lake surface extents based on NDWI threshold segmentation in order to investigate the surface area variations of the nine most important lakes in Central Asia in 1975, 1990, 1999, and 2007. During 1975–2007, the combined water surface extents of the nine lakes declined from 91,402.06 km² to 46,049.23 km², representing a loss of 49.62 % to their entire extent in 1975.

Sisay (2016) used Landsat images data to detect and quantify the water surface extent variations of Lake Shala, Abjata, and Langano in Ethiopia's Central Rift Valley Region between 1973 and 2014 by employing the NDWI and AWEI. The results indicate that Lake Shala and Lake Langano have seen negligible changes -3.68 km² and -10.2 km² respectively, compared to Lake Abjata -68 km² between 1973 and 2014, which makes Lake Abjata, the lake that its surface area has changed the most dramatically.

Based on Buma et al. (2018), the *M*NDWI was a valuable index for mapping water surface area changes in Lake Chad, with an overall accuracy of around 96%. Thus, the index was used to determine the lake's surface area changes from 2003 to 2016. Xia et al. (2019) analyzed the satellite data on the GEE platform using the available 16,760 scenes of Landsat images, utilizing a combination of vegetation indices NDVI and Enhanced Vegetation Index (EVI) and the water index *M*NDWI in order to detect the changes in water surface extents of the Huai River Basin from 1989 to 2019. The results show that the maximum, average, and seasonal changes in surface water extents

in the basin exhibited a decreasing trend, while the annual surface water extent exhibited a modest upward trend with overall accuracy of 93.6%.

Wang et al. (2020) employed all available Landsat images (7534 scenes) in order to comprehend the long-term changes of the surface water extent in Hetao Plain, and they adopted the NDWI, *M*NDWI, EVI, and NDVI to map the open-surface water from 1989 to 2019 on the GEE cloud platform. They analyzed the variation of water surfaces over a period of 32 years and determined the pattern of change by analyzing the area and some various water bodies. The results show that with an overall accuracy of indices was 95.9%. While, the maximum, seasonal, and annual average water surface area demonstrated a general tendency of decrease, whereas the maximum, seasonal, and permanent water surface number exhibited an overall rising trend.

Soltani et al. (2021) used Landsat satellite images and a stochastic method to figure out the surface area of Lake Gregory in Australia. The using of NDVI, NDWI, and MNDWI indices was examined to obtain the surface water maps of the lake, the detected pixels of satellite images have been separated into water and non-water categories. The overall trend data from 2004 to 2019 indicates that the lake's surface area is progressively decreasing, reaching its smallest area in 2019.

1.2.1.1 The used of satellite data and remote sensing indices in Türkiye’s natural lakes

In the last 40 years, half of Türkiye's inland water bodies have lost their ecological and economic features due to drying, filling, and interference with water systems (WWF, 2008). Inappropriate irrigation practices, huge pollution, illegal hunting and fishing, and other large-scale investments including highways are among the primary causes of the decrease in Türkiye's inland water bodies. Unplanned water projects such as dams built on rivers and feeding lakes are another major threat (Dervisoglu, 2021).

Research on Türkiye's natural lakes utilizing remote sensing data and indices has been done.

Based on Akşit (2014), by analyzing satellite images, it was indicated that Lake Burdur had shrunk by 65.98% in the previous two decades. When the majority of water extraction structures were built between 1987 and 2000, the water area dropped by 22.68%, and the region shrank by 14.63% between 2000 and 2010. They also indicated

that the drop in the area between 1987 and 2000 may have been mostly the result of dams, but the loss between 2000 and 2010 might be primarily the result of drought.

By using Landsat TM data from 1984 and 2013 and Terra Advanced Spaceborne Thermal Emission and Reflection Radiometer (ASTER) satellite data from 2004-2005, and then topographic maps were converted into raster data, Fethi et al. (2015) calculated the surface area of Lake Beysehir and Lake Egirdir. The shorelines of both lakes were vectorized using Erdas and Geographic Information System (GIS) software. The results show that Lake Beysehir had a surface water extent of 652 km² in 1984, and it was 639 km² in 2014. While, the surface extent of Egirdir Lake was 463 km² in 1984, 458 km² in 2004, and it was assessed to be 454 km² in 2013.

According to Sarp and Ozcelik (2017), Landsat images were used to assess the changes that occurred in Lake Burdur's surface area from 1987 to 2011. The surface water of the lake was extracted from Landsat images data using spectral water indexing, including the NDWI, MNDWI, and AWEI. The results indicated that from 1987 to 2000, the lake lost around 1/5 of its surface area relative to 1987, and between 2000 and 2011, it lost about 1/10 of its surface extent compared to 2000.

Yagmur et al. (2018) evaluated the temporal variations of the lentic water surfaces in the Konya Closed Basin at every 5 years interval between 1987 and 2017 using Landsat image data within the GEE platform. The NDWI was used to determine the surface area changes of water bodies. The findings revealed that throughout the course of the 30-year inspection period, water surface areas had reduced by roughly 22.5 %, Tuz Lake has shrunk by approximately 46%, and Beysehir Lake has shrunk by only 2.4 %.

Gozukara et al. (2019) found that the Burdur Lake level decreased by 13.74 m (-2%) and the lake surface area decreased from 211 km² to 130 km² (-38.39%) during 42 years (1975-2017) by using Landsat imageries. When examining the link between the water level of Burdur Lake and meteorological data, it was discovered that the temperature of -0.637 and total evaporation of -0.603 had the largest correlation with the lake's level decline.

Dervisoglu (2021), assessed the temporal changes in Türkiye's inland Ramsar sites using Landsat satellite images and the NDWI. It found that inland wetlands declined at varying rates between 1985 and 2020, totaling 31.38% and 21,571 hectares in the

spring months. Since then, the total amount of water surface area has reduced by 27.35%, representing 17,758.90 hectares.

Moreover, according to Abujayyab et al. (2021), they collected 570 Landsat images from GEE for the surface area of Burdur Lake during a period between 1984 and 2019, where a seasonal fluctuation in the area of water bodies was determined by combining their suggested extraction technique using NDWI. The lake's entire extent decreased from 206.6 km² in 1984 to 125.5 km² in 2019.

1.2.2 Lake Surface Water Temperature (LSWT)

Traditional techniques for measuring water surface temperature are costly and time consuming. Instead, remote sensing data could expedite and reduce the cost of this operation. Land Surface Temperature (LST) and LSWT studies commonly use Landsat images, which are among the most widely utilized types of remote sensing data.

The LSWT refers to the temperature of the lake's surface water, which is a critical indication of the lake's hydrology and biogeochemistry. Temperature patterns throughout time could provide insight into how climate change is affecting the lake’s surface area. A relationship existed between the extent of lake surface area lost and the rise in LSWT measurements (Aslan and Koc-San, 2021). There is a substantial positive or negative relationship between the reduction of surface water area and the meteorological factors including temperature, thus according Abujayyab et al. (2021), the research was concluded that remote sensing can be used to identify the impacts of climate change on lakes. Moreover, climate change has a negative impact on water bodies in Türkiye and the rest of the world (Gorguner and Kavvas, 2020).

Over the last century, the average global surface temperatures have increased, and it is predicted that future climate change would have a negative impact on aquatic ecosystems (URL 1). Water temperatures are rising dramatically in lakes around the world, and this trend is likely to have a negative impact on aquatic ecosystems (O’Reilly et al, 2015). As a result, several studies on lake’s water temperature have been conducted.

According to Xie et al. (2022), MODIS lake surface temperature data were employed to determine the spatio-temporal changes in LSWT of China's large lakes between 2001 and 2016. Their findings indicated that the 169 large lakes included in the study

had an overall increasing trend in LSWT, with an average rate of 0.26 °C/decade. With overall of 121 lakes (71.6%) had an increase in daytime temperature at a mean rate of 0.38 °C/decade, whereas 48 lakes (28.4%) experienced a decline at a mean rate of 0.21 °C/decade. The correlation analysis of LSWT trend and air temperature trend for each lake indicated that, for the majority of lakes, LSWT was positively linked with daytime and nighttime air temperature trends.

Based on Aslan and Koc-San (2021), in the years of 1998, 2008, and 2018, the surface lake area and LSWT of Burdur and Egirdir Lakes were analyzed using Landsat satellite images, as well as the correlations between these parameters. The NDVI and MNDWI were used to extract the shoreline of the two lakes. Thus, after a 20-year period, it was found that the increase in LSWT values was about 2.2°C for Burdur Lake and approximately 1.3°C for Egirdir Lake, while both lakes' water surface area decreased.

2. REMOTE SENSING

Based on measuring a region's reflected and emitted radiation, remote sensing is a method for detecting and tracking its physical characteristics from satellite or aircraft. Specialized cameras on satellites or airplanes capture remotely sensed images, which researchers use to sense aspects of the Earth (URL 2).

Through remote sensing technology, information extraction is an efficient and beneficial way for almost all fields. There are several approaches for extracting information from satellite images, including visual interpretation, digitization, classification algorithms, and algebraic operations such as spectral indices. Thus, NDWI is one of the spectral indices, which is used in our study to detect water pixels in order to determine the water surface area as explained in the previous chapter.

2.1 Remote Sensing of Water Surfaces

Using remote sensing, one could effectively examine surface water dynamics. It is significantly more efficient than conventional in situ measurements since it can continually monitor the Earth's surface at different scales. Remote sensing data sets enable spatially precise and temporally frequent observations of a range of physical features of the Earth's surface that can be used to map the extent of water bodies on a regional or even global scale and to monitor their dynamic changes on a regular basis. Satellite imagery is utilized to assess the temporal and spatial changes in water resources, and monitoring these changes using satellite imagery enables quicker and more effective findings than conventional approaches (Kale and Acarlı, 2019).

The use of satellite images to assess spatial and temporal changes in the water surface of lakes has grown more important across the world. Remote sensing technologies have made the manual mapping of surface water simpler and quicker. Thus, images that are captured by remote sensing satellites or airborne sensors, include a lot of information that can be accessed, analyzed, and examined using digital image processing methods, throughout the years a number of straightforward and efficient water mapping techniques have been created.

There are several uses for remote sensing imaging, including agriculture, food processing, mineralogy, and environmental investigations. The concept of using multi-spectral images to extract water surfaces is driven by the fact that water has a very distinctive spectral signature in the electromagnetic spectrum. The majority of multispectral sensors record images in the visible, near-infrared, and infrared regions of the electromagnetic spectrum. The spectral signature of water seen in Figure 2.1 demonstrates conclusively that NIR and infrared bands could be highly beneficial for researching water bodies.

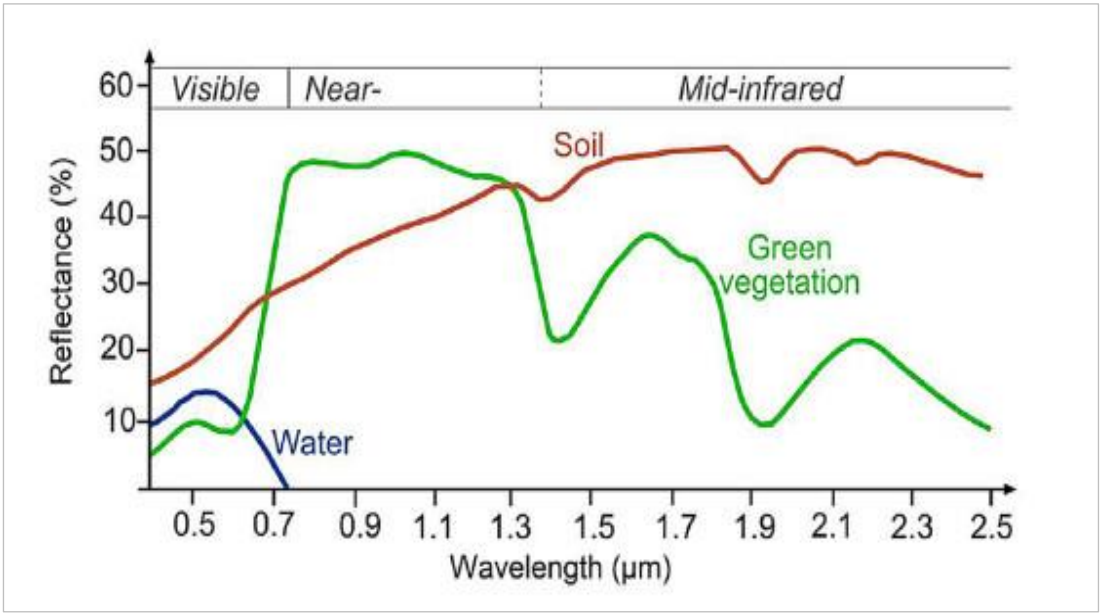

Figure 2.1 : Spectral characteristics of water, soil, and vegetation (Lillesand et al, 2015).

The majority of the satellites that have been launched, capture images of the scene in the visible, NIR, and SWIR portions of the electromagnetic spectrum, which makes them appropriate for use in applications involving surface water mapping.

The Landsat satellite series is ones of the most successful one in history. Since the first mission was launched in 1972, it has consistently provided images with a high resolution. Landsat 5 sensor has served for an unexpectedly long time, which has led to widespread use of Landsat TM images for surface water monitoring since 1984. The Landsat 8 sensor, which was launched in 2013, is the most current Landsat satellite, although its OLI data are already frequently utilized for detecting surface water (Huang et al, 2018).

3. STUDY AREA AND SATELLITE DATASETS

3.1 Study Area

Türkiye's inland water bodies represent around 1.6% of the country's geographical area, and the 200 natural lakes encompass over 906,000 hectares (WWF, 2008). The General Directorate of Nature Conservation and National Parks (GDNCNP), which belongs to the Ministry of Agriculture and Forestry (MoAF), manages 302 different lakes and wetlands with surface areas ranging from 8 to 352,269 hectares (Firatli et al, 2022).

The study area is located in the Lakes Region, which is situated in the Mediterranean region of Türkiye between latitudes N 37° 01' and N 38° 30' and longitudes E 29° 33' and 32° 21' as shown in Figure 3.1. In this region, the elevation varies between 800 and 1500 meters. The Lakes Region is formed of basins, with the western part of the region consisting of one more closed basin, the most significant of which being Lake Burdur, and the eastern part, which includes Lake Beysehir. The Aksu River links the center part of the region to the Mediterranean Sea, which empties excess water from Lake Egirdir. The basins of the Lakes Region are predominantly the result of karstic topography and tectonic processes, which is the Mediterranean Transitional ecoregion.

The major three of these lakes were selected for our study in order to examine the changes that occurred in their extent during a 21-year period from 2000 to 2021, including: Lake Burdur (brackish), Lake Egirdir (freshwater), and Lake Beysehir (freshwater). The climate is dry and hot in the summer, cold in winter, and wet in the spring, with an average yearly temperature of 11° to 14° C at 1000 meters (Atalay and Efe, 2008). However, the lowest temperature was 3.5 °C in Goksun and the highest temperature was 46.1 °C in Koycegiz during 2021. The mean annual precipitation is 666.5 mm, and it was 726.9 mm in 2020. There was a 24% decrease in precipitation compared to normal, and a 30% decrease compared to 2020 precipitation. (Turkish State Meteorological Service, 2021).

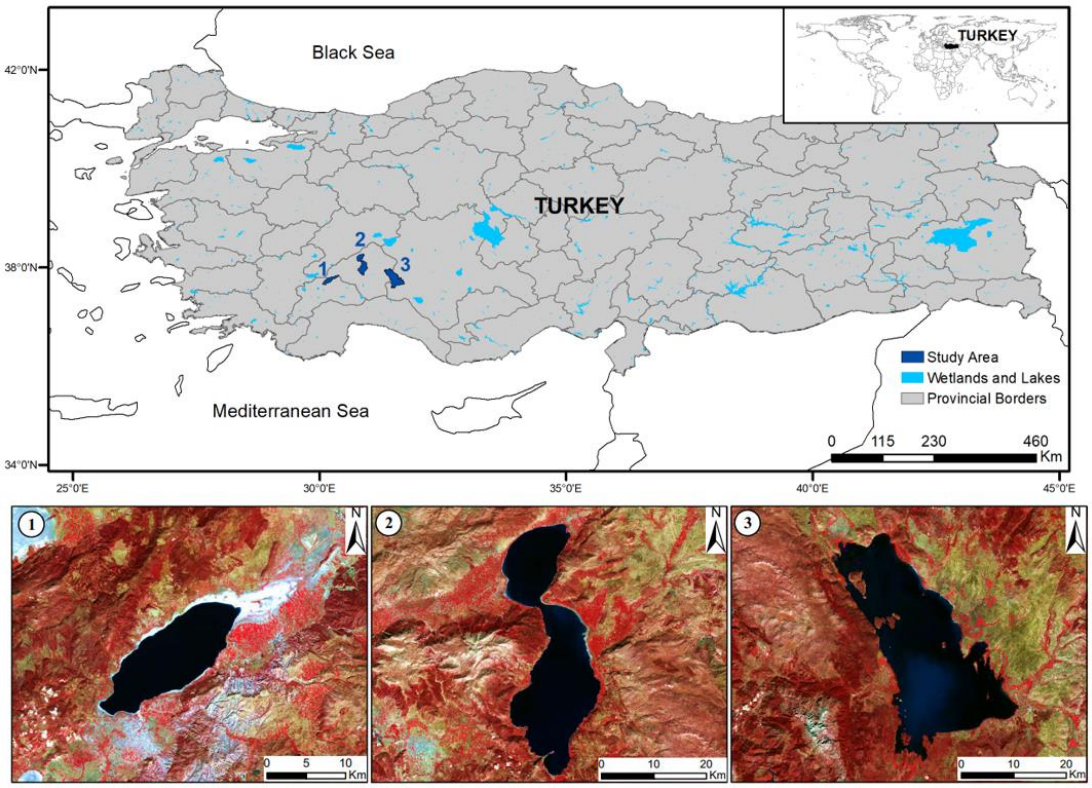

Figure 3.1 : The Study Area's Location Map, (1) Lake Burdur, (2) Lake Egirdir, and (3) Lake Beysehir.

Burdur Lake: A pier at the seventh biggest lake in Türkiye, it is a salty lake produced by tectonic activity and it is unsuitable for irrigation and the lake situated in Burdur and Isparta provinces. The lake is supplied by rainwater from the surrounding watershed, which covers an area of 3211 (Bostan, 2017). Nearly 100 bird species may be seen at Lake Burdur, which has been a Ramsar Site since 1993 and a Wildlife Reserve since 1994 (URL 3). It has decreased in water level and area rapidly in recent years. Because of that, the habitat that relies on it is under jeopardy.

Egirdir Lake: It is a freshwater lake which is located in the Isparta region that was created by geological and karstic forces. Along with serving as drinking water basin, it is a globally significant wetland for its biological benefits. The lake has been designated as a natural area and it hosts 91 plant species and more than 150 kinds of birds.

Beysehir Lake: The third biggest lake in Türkiye. It is a freshwater lake and it is situated in the province of Konya, Türkiye. A tectonic setting surrounds the lake (Cevik, 2009). In 1992, the lake was designated as a natural protected area. It is used

for irrigation and domestic purposes, and it is considered to be an important site for many bird species.

The maximum extent, elevation, maximum depth, and other related properties of the assessed lakes are shown in Table 3.1.

Table 3.1 : Various properties of study lakes (URL 4).

Lake	Maximum Extent (km^2)	Type	Maximum Depth (m)	Elevation (m)	Purpose of Use	Protection Status
Burdur	195.37	Brackish	100	857	-	Ramsar Site
Egirdir	476.92	Freshwater	15	917	Irrigation	Natural protected area, Drinking water reservoir
Beysehir	706.46	Freshwater	15	1124	Drinking water, Irrigation	Natural Park, wetland Protected area, Drinking water reservoir

3.2 Satellite Data

Various satellite sensors were used in this study, including Landsat 5 TM and Landsat 8 OLI/TIRS, to cover as much of the study period as feasible from 2000 to 2021. Landsat 5 TM provides coverage from 2000 to 2011, and Landsat 8 OLI/TIRS provides coverage from 2013 to 2021. The GEE cloud platform was employed to query and analyze all these image sets.

3.2.1 Properties of Landsat TM and OLI/TIRS sensors

In the electromagnetic spectrum, remote sensing devices measure an area's brightness. Spectral sensitivity intervals (bands) are used to describe the spectral resolution of all sensors. Landsat's sensors were designed to capture data across a broad range of electromagnetic frequencies. Figure 3.2, shows a comparison of Landsat spectral bands. While Landsat instruments are basically simple electro-optical transducers that consume photons and emit a digital bit stream, they rely on cutting-edge technology

in a variety of areas, including optics, precise electro-mechanics, detectors, sophisticated materials, cryogenics, and signal processing.

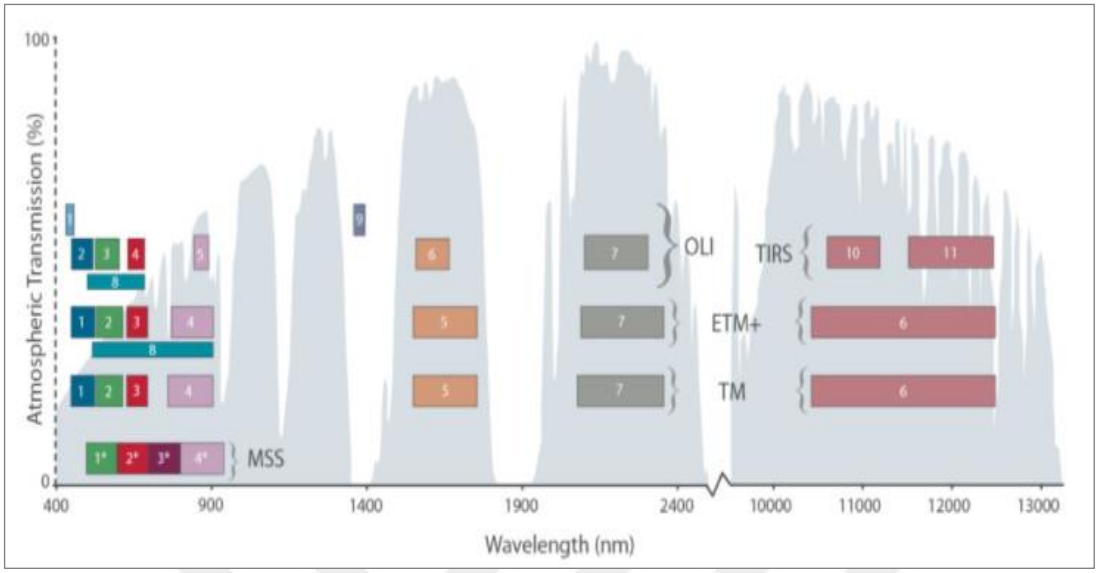

Figure 3.2 : Visual comparison of Landsat spectral bands (URL 5).

In this study, Landsat 5 TM, and Landsat 8 OLI/TIRS imagery were used. Landsat images are often used in environmental research because of their low cost and great temporal resolution. Landsat 5 TM is equipped with six multispectral bands and one thermal band. While, Landsat 8 OLI/TIRS images include eight multispectral bands, one panchromatic band, and two thermal bands. It has radiometric resolutions of 8 and 16.

The TM is a sophisticated multispectral scanning earth resources sensor developed to generate better image resolution and more radiometric accuracy and resolution than the Multispectral Scanner (MSS) sensor. Landsat 5 has a thematic mapper sensor. It has a spatial resolution of 30 m, which is the smallest item that the sensor can discern. The sensor has a spectral range of 0.45 to 12.5 m and a temporal resolution of 16 days. Bands 1 to 5 and 7 of Landsat 5 TM images have a spatial resolution of 30 m. The spatial resolution of Band 6 (thermal infrared) is 120 m, but is down sampled to 30 m. The approximate extent of the scene is 170 km north to south by 183 km east to west. In bands 1-5 and 7, the Instantaneous Field of View (IFOV) of a TM scene is 30m by 30m, whereas the IFOV on the ground is 120m by 120m in band 6 (URL 6).

The OLI sensor measures the visible, NIR, and SWIR portions of the spectrum. Along a 185 km (115 mile) broad swath, sensor’s images feature 15m panchromatic and 30m

multispectral spatial resolutions. The Landsat TIRS collects image data for two thermal infrared spectral bands with a spatial resolution of 120 m across a 185 km swath. The two bands were selected to provide atmospheric correction of the thermal data and constitute an improvement over the single-band thermal data gathered by previous Landsat satellites. Landsat 8 is equipped with OLI/TIRS sensors. The Landsat 8 thermal bands (bands 10 and 11) produce the correct surface temperatures and they are collected at a height of 100 m (URL 6). Table 3.2 lists the resolution features of the TM and OLI/ TIRS sensors.

Table 3.2 : The Spectral and Spatial Resolutions of TM & OLI/TIRS sensors (URL 6).

	TM (Landsat 5)			**OLI/ TIRS (Landsat 8)**		
Band	Band Description	Spectral Resolution (μm)	Spatial Resolution (m)	Band Description	Spectral Resolution (μm)	Spatial Resolution (m)
1	Blue	0.45-0.52	30	Coastal Aerosol	0.435 - 0.451	30
2	Green	0.53-0.60	30	Blue	0.452 - 0.512	30
3	Red	0.63-0.69	30	Green	0.533 - 0.590	30
4	Near Infrared (NIR)	0.77-0.90	30	Red	0.636 - 0.673	30
5	Shortwave Infrared (SWIR) 1	1.55-1.75	30	Near Infrared (NIR)	0.851 - 0.879	30
6	Thermal	10.40-12.50	60	Short-wave Infrared (SWIR) 1	1.566 - 1.651	30
7	Shortwave Infrared (SWIR) 2	2.09-2.35	30	Short-wave Infrared (SWIR) 2	2.107 - 2.294	30
8				Panchromatic	0.503 - 0.676	15
9				Cirrus	1.363 - 1.384	30
10				TIRS 1	10.60 – 11.19	100
11				TIRS 2	11.50 - 12.51	100

3.2.2 ERA5-Land and TerraClimate monthly satellite dataset

To show whether there is correlation between water surface area and LSWT with meteorological parameters (temperature, evaporation and precipitation), ERA5-Land and TerraClimate monthly satellite datasets were used in this study. The ERA5-Land dataset is produced from ERA5 land variables with enhanced resolution. The process steps consist of modelling data using consistent global observations considering laws of physics and providing data (50 variables) since 1981 with approximately 11 km spatial resolution. Monthly data is also produced by taking average of hourly collected data (URL 7).

The other dataset is the TerraClimate monthly dataset. TerraClimate dataset is produced by combining interpolated time-varying data CRU Ts4.0 and the Japanese 55-year Reanalysis (JRA55) with high spatial resolution WorldClim dataset. Unlike ERA5-Land, TerraClimate has nearly 5 km spatial resolution and 14 variables between the years 1958 and 2021 (URL 8) Both of the datasets exist in the database of the GEE cloud platform and data was retrieved from the GEE database for the study area.

4. METHODOLOGY

This chapter details each phase of the thesis writing process. It is demonstrated with explanations including the equations and GEE code. The flowchart of the methodology is shown in Figure 4.1.

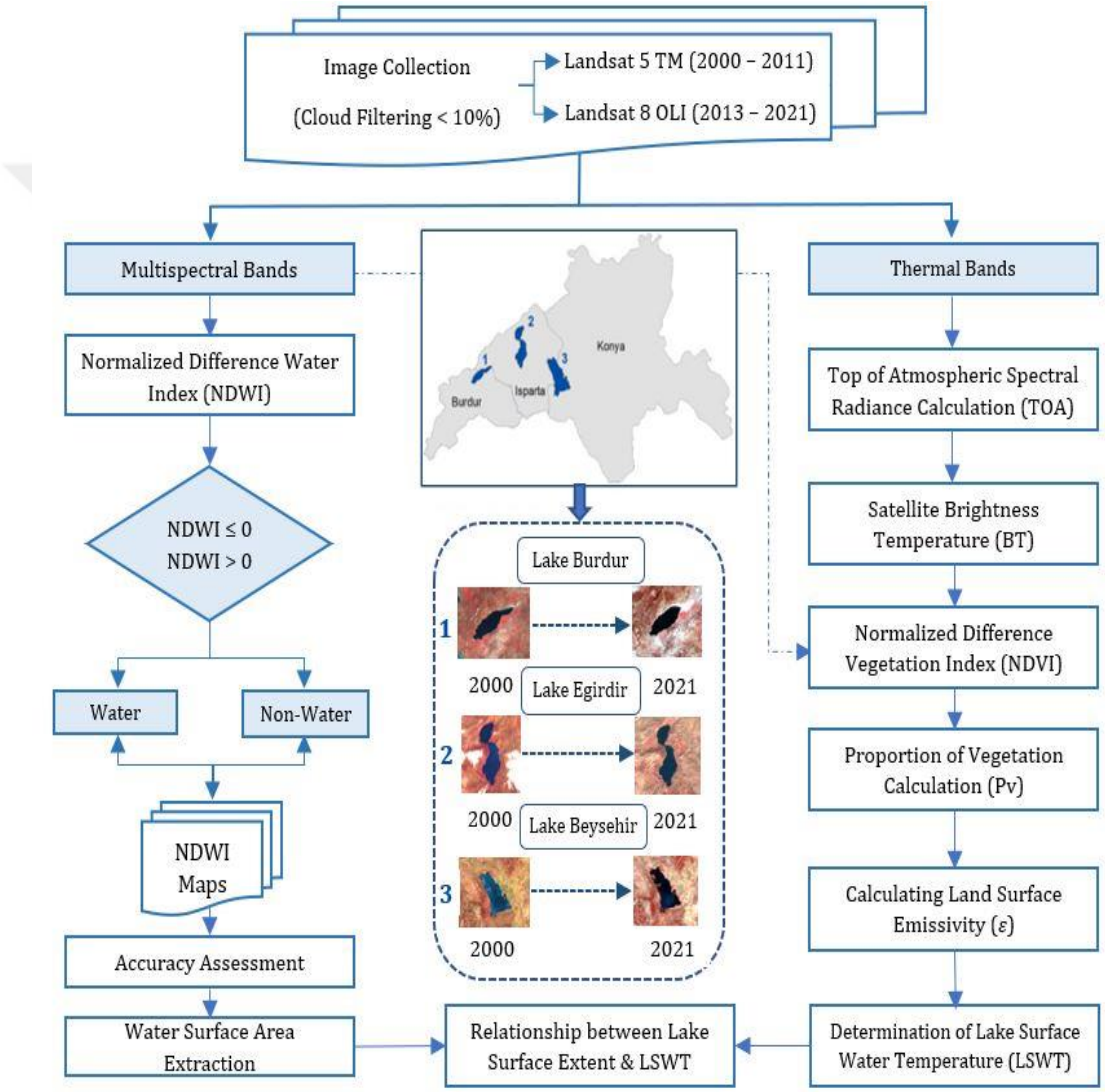

Figure 4.1 : The methodology's flowchart.

The GEE permits the filtering and elimination of low-quality images produced by shadows, snow, and clouds. Thus, all collected images were masked according to the research study area. The time series continuity is improved by analyzing as many images as possible. As a result, multiple Landsat tiles were discovered mostly overcast

but not cloudy inside the study region of each lake during the analysis of the Landsat images. Therefore, these Landsat tiles were used to maintain the derived time series continuity. The number of images utilized for each study lake is shown in Table 4.1.

Table 4.1 : Number of images used for each lake.

Lakes	**Landsat 5 TM (2000-2011)**	**Landsat 8 OLI/TIRS (2013-2021)**	**Total**
Burdur	161	158	319
Egirdir	76	70	146
Beysehir	74	67	141
Total	311	295	606

In this research, all accessible imagery from the years 2000 to 2021 except 2012, for which there were no available images covering the study area in that year, was used to examine the dynamic behavior of water surface extents at finer temporal scales with a total of 606 Landsat images, as seen in Figure 4.2, which shows the distribution of used images for each year during the study period. Previous researches (Gulcan and Sarp 2016; Dervisoglu 2021; Abujayyab et al. 2021; Firatli et al. 2022) have used the short- and long-term in monitoring the changes occurred in water surface area of the lake. Due to describe long-term patterns of surface water fluctuation, many years of images must be captured at the same time, which might lead to inconsistent regions of surface water and uncertainty in the results.

Moreover, choosing an ideal time to acquire satellite images may be challenging for a variety of reasons. Thus, using all accessible images through a year aims to avoid these mapping difficulties, discrepancies, and ambiguity. Consequently, comprehensive research is required to ascertain the ongoing change of surface water regions by utilizing adequate images acquired over several seasons and years.

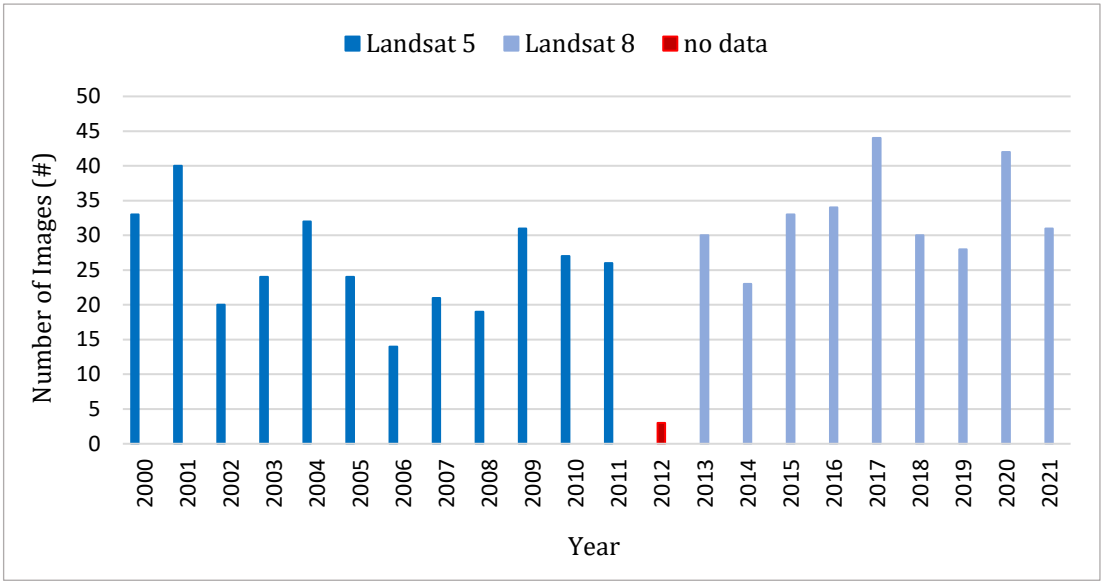

Figure 4.2 : The number of used satellite images for each year.

In the study, the image download technique was not appropriate since all satellite images were to be used within the specified time frame. Landsat 5 TM images from 2000 to 2011 were utilized in this thesis. The 311 Landsat 5 TM images available for the three lakes were detected by applying 10% cloud filter. More than 100 megabytes (MB) is the size of a single Landsat 5 TM image, which will be downloaded from the USGS website. Therefore, it would need around 30 Giga-Bytes (GB) of storage space that cover all the study lakes between 2000 and 2011. For the period from 2013 to 2021, 295 Landsat 8 OLI/TIRS images were analyzed. The image of a Landsat 8 OLI/TIRS is more than 900 MB in size. Thus, 265 GB of storage space would be required if they were downloaded from the USGS website.

If all the images included in the thesis were downloaded, roughly 295 GB of Landsat data would be stored. Depending on your connection speed, downloading these images may take up to 3 days. Furthermore, using a home computer to process these 606 images would take a long time. It would be wasteful and unproductive due to the data storage and processing time. Consequently, the analyses in this study were completed in a matter of minutes using the GEE cloud platform without the need to download any images.

4.1 Lake Water Surface Area Calculation Using GEE Platform

Google Earth Engine is a cloud-based computing platform that allows the execution of geospatial analysis on Google's cloud infrastructure. A web-based Integrated

Development Environment (IDE) is utilized for creating and executing scripts (Figure 4.3). Additionally, this IDE is utilized to visualize geographical studies through the JavaScript application programming interface (API). The GEE libraries could be used to build JavaScript and Python programs (URL 9).

The GEE data catalog contains a large collection of publicly accessible geospatial datasets, including observations from a wide range of satellite and aerial imaging systems at optical and non-optical wavelengths; environmental variables; weather and climate forecasts; land cover; topographic; and socioeconomic datasets. All this data is pre-processed to an accessible but information preservation state that allows efficient access and avoids several difficulties connected with data management (Gorelick et al, 2017). All the analysis mentioned in Sections 4.1.1, 4.1.2, 4.1.3, and 4.1.4 was carried out through the writing of codes in an IDE using the GEE cloud platform.

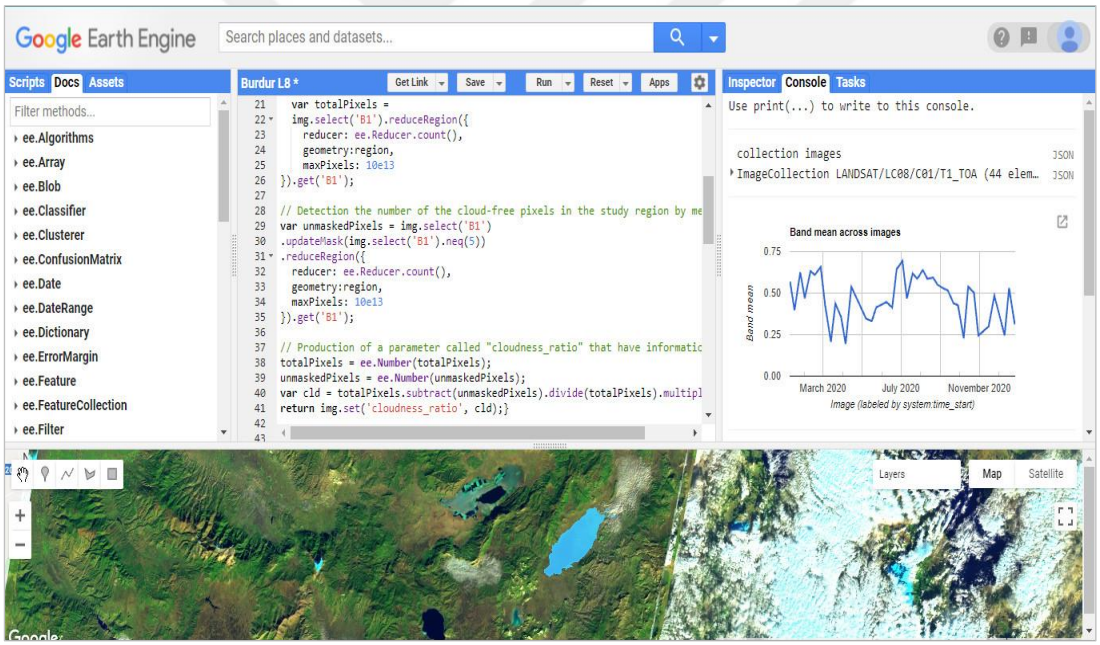

Figure 4.3 : A view of the GEE code in conjunction with the Code Editor.

4.1.1 Selection of image collection used in analyses and apply the cloud filtering

In the first stage of analysis of spatio-temporal changes in lake water surface area calculation, all related Landsat images were selected and listed throughout the GEE database within the lake boundaries for each lake. Separate folders and codes were generated for Landsat 5 TM and Landsat 8 OLI/TIRS images. The date range was from 2000 to 2021, an image collection was made depending on this filter. Which are consider to serve as the foundation for the analysis in this study.

After collecting image collections based on date filtering, it was intended to compute water surface areas within this collection of images. However, cloud filtering must first be implemented to the images, since clouds prevent the pixels from being categorized as water. Images with a cloud ratio of less than 10% were included in the study, while the others were discarded. Each satellite image's metadata includes cloud coverage information. Cloud filtering was performed exclusively in the regions specified in the GEE codes. Following this procedure, image collections with the required level of cloudiness were produced for the specified time period (2000–2021). Thus, only the lake analysis borders were examined in this study.

The following is an example of GEE code that enables the selection of image collection from Landsat 8 sensor by applying cloud filtering for Lake Burdur:

- The lake boundaries in shp. format imported from local computer:

```
var region = ee.FeatureCollection("exmaple/BurdurLake");
```

- Selection of the satellite and image filtering:

```
var l8images = ee.ImageCollection('LANDSAT/LC08/C01/T1_TOA')
                    .filterDate('2013 - 01 - 01', '2021 - 12 - 31')
                     .filterBounds(region)
                    .filter(ee.Filter.lt('CLOUD_COVER', 10));
```

4.1.2 Normalized Difference Water Index (NDWI) Calculation

Image collections from Landsat 8 OLI/TIRS and Landsat 5 TM satellites with less than 10% cloudiness ratio through the analysis boundaries of the lakes were acquired during the study period. These sets include almost 606 images. One of the most critical aspects of this thesis is the ability to identify and visualize water pixels inside the analysis boundaries.

The NDWI was chosen as one of the indices for detecting water category in the images according to related bands in each sensor. McFeeters (1996) developed the NDWI, which maximizes water reflection in the green band while minimizing water reflection in the NIR band, and exploit the high NIR reflectance of terrestrial vegetation and soil characteristics. (Equation 4.1). The NDWI has the ability to provide researchers with turbidity analyses of water bodies using remotely sensed digital data. Consequently,

Water properties have positive values and are therefore enhanced, while vegetation and soil usually have zero or negative values and are thus discarded. It is simple to configure image processing through GEE to eliminate negative values. This efficiently removes the information about terrestrial vegetation and soil, while retaining the information about open water for study. Thus, the range of NDWI is from -1 to 1 (McFeeters, 1996; Xu, 2007).

$$NDWI = \frac{(Green\ band - NIR\ band)}{(Green\ band + NIR\ band)} \quad \textbf{(4.1)}$$

To calculate the NDWI threshold for detecting water and non-water pixels, it has been scanned within the duration of the related sensor chosen satellite image for each lake. The threshold value of zero was suggested for extracting surface water pixels with all positive NDWI values classed as water and all negative NDWI values, including zero, classified as non-water (McFeeters, 1996). The same satellite images were utilized to establish the accuracy for the smallest and largest water surface areas, which were recorded depending on NDWI.

After establishing a NDWI zero threshold, a set of GEE API scripts was created to generate a time series of lake water surface areas for each lake using all the images from the image collections. The GEE algorithm for determining the water pixels using NDWI thresholding from Landsat 8 as an example is shown below.

- Add the NDWI bands (Green and NIR) then get pixels above the threshold

```
var waterfunction = function(image) {
var ndwi =image.normalizedDifference(['B3','B5']).rename('NDWI').clip(region);
var water01 = ndwi.gt (0)
```

- Extract only the water pixels

```
image = image. addBands (ndwi).updateMask (water01)
```

- Application of the function to all image collection

```
var l8ndwi = l8images.map (waterfunction).Select ('NDWI')
```

4.1.3 Accuracy assessment of NDWI maps

The purpose of this section is to demonstrate the accuracy of the proposed surface water pixels extraction technique and to verify the quality of the lake boundary extraction data. To determine the accuracy assessment of the NDWI zero threshold in

GEE for each lake, the NDWI image was clipped to the boundaries, and then the images that have the smallest and largest lake surface area were downloaded. By using ArcGIS software, random points were selected for each NDWI lake map and compared with the lake Landsat image to verify whether the accuracy point is in the water or not. Thus, a total of 318 points were selected randomly for Lake Burdur, 403 points for Lake Egirdir, and 495 points for Lake Beysehir, as seen in Figure 4.4 an example for the largest surface area of Lake Burdur, Egirdir, and Beysehir.

A confusion matrix as shown in Table 4.2 was generated to compute the Producer Accuracy Equation (4.2), User Accuracy Equation (4.3), and Overall Accuracy Equation (4.4), and Kappa Coefficient Equation (4.5). The matrix, also referred to as the error matrix, is a comparison array that is used to represent the number of pixels classified into a certain category. It has been extensively used to evaluate the classifying accuracy of remote sensing images.

In the confusion matrix, each column represents a predicted water or non-water category, and the total number in each column denotes the number predicted for that category (Producer); each row represents the true attribution category of the data, and the total amount of data in each row represents the real number of the category (User). Where the Overall Accuracy is defined as the percentage of test samples categorized properly by the model, that is the number of samples classified correctly divided by the total number of test samples. The Kappa coefficient has been developed as a technique for controlling for the random agreement component. Typically, kappa values vary from 1 to +1, where 0 denotes the predicted degree of agreement from random chance, and 1 denotes full agreement between raters (Mchugh, 2012).

When comparing the extracted water and non-water map with the reference data, four categories of pixels are identified:

I. TP: True positive value;
II. FP: False positive value;
III. FN: False negative value; and
IV. TN: True negative value.

Table 4.2 : The confusion matrix (Stehman, 2014).

		Reference Data	
		Water	**Non-water**
Classified Data	Water	TP	FP
	Non-water	FN	TN

$$Producer's\ Accuracy = \frac{TP}{TP+FN} * 100 \quad \textbf{(4.2)}$$

$$User's\ Accuracy = \frac{TP}{TP+FP} * 100 \quad \textbf{(4.3)}$$

$$Overall\ Accuracy = \frac{TP+TN}{Total\ Number\ of\ Pixels\ (T)} * 100 \quad \textbf{(4.4)}$$

$$Kappa\ Coefficient = \frac{([T*(TP+TN)]-\sum(Column\ Total \times Row\ Total))}{T^2-\sum(Column\ Total \times Row\ Total)} * 100 \quad \textbf{(4.5)}$$

Producer Accuracy, User Accuracy, and Overall Accuracy all reflect accurate predictions and have a range of 0 to 100%, when the value close to 100% indicating perfect accuracy.

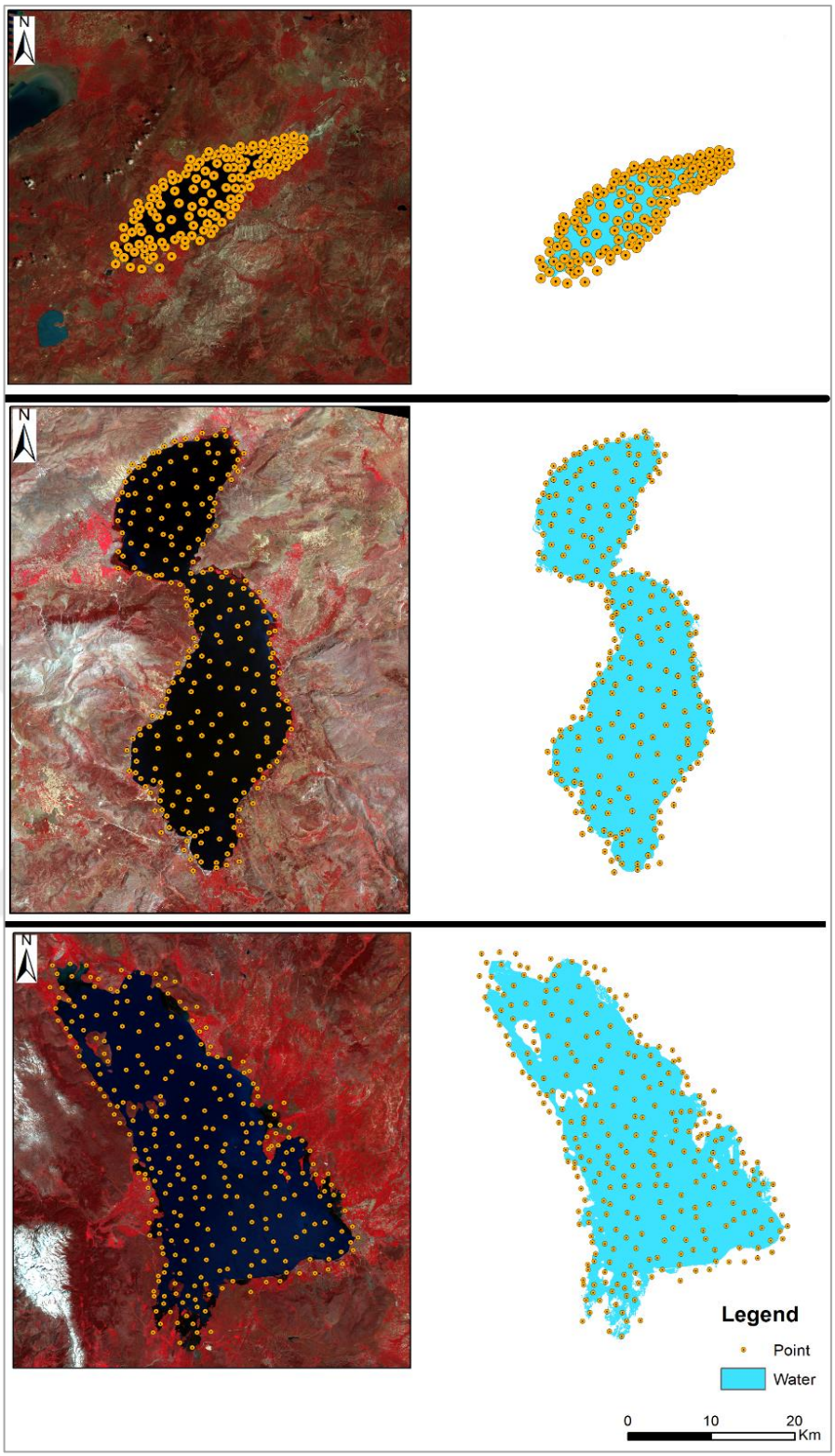

Figure 4.4 : Accuracy assessment using random point selection method for the largest water surface.

4.1.4 Lake water surface area calculations

Once water pixels were detected inside the analysis borders, it was needed to compute the water surface area corresponding to the water pixels that had been detected.

To avoid obtaining values for the lake water surface area that are lower than the average area, an average filter was used. The filter was set to more than 100 km² for Burdur lake, greater than 430 km² for Egirdir lake, and greater than 500 km² for Beysehir lake.

A GEE code was used to calculate the water pixels area, these operations are shown below as an example for Lake Burdur.

- Change all water pixel values to 1 then multiply by ee.Image.pixelArea; since that image gives us the area of each pixel:

```
var waterArea = water01
                    . divide(water01)
                    . multiply(ee.Image.pixelArea())
                    . rename('waterArea')
                    . divide(1e4);
```

- Adding area of water as a band:

```
image = image. addBands(waterArea);
```

- Calculate water surface area:

```
var stats = waterArea.reduceRegion({
            reducer: ee.Reducer.sum(),
            geometry: region,
            scale: 10})
return image.set(stats)
```

- Average lake surface area filter depending on the average lake area to avoid the lower values (100 km² for Lake Burdur):

```
var filterarea = collectionarea.filter(ee.Filter.gt ('waterArea', 100))
```

4.2 Displaying Surface Water Area Time Series for each Lake

The API of GEE includes a function that allows the creation of time series charts from image collections. Although this function only shows the dates with imagery, the time intervals between the Landsat collected images dates are not effectively represented as a consequence of the limitations of this function. So, bar charts in Microsoft Excel were used to display the total number of days between 2000 and 2021, with or without accompanying images. In GEE, a time series of water surface area was produced and

imported into Microsoft Excel to display the results. Afterwards, the dates devoid of images were added to the collection.

Moreover, the seasonal variations that occurred in the water surface extent of each lake between 2000 and 2021 were analyzed and calculated. The bars in each graph, which represent computed water surface area on related season with less than 10% cloud cover. The Landsat imageries for years 2000, 2011, and 2021 were added to show the spatial changes that occurred during the study duration. An empty bar means there is no image or cloud-free image on the given season. For each satellite, a different color is used for the bars. Additionally, the long-term annual water surface area variations with respect to year 2000 were analyzed to present the percentage of changes in surface area, whether they recovered or decreased in the relevant year.

4.3 Lake Surface Water Temperature (LSWT) Calculations

In this section, the LSWT data for the three lakes was calculated using Landsat 5 TM and Landsat 8 OLI/TIRS thermal bands. Where Landsat 5 TM has just one thermal band: the 6th band. On the other hand, for Landsat 8 OLI/TIRS there are two thermal bands: the 10th and 11th bands to show the changes of LSWT. However, this research used just the 10th band since it was advised to deal with TIRS band 10 data as a single thermal band.

The average values of LSWT for the summer and autumn seasons between 2000 and 2021 were assessed and retrieved using the NDWI map of 2000 to demonstrate the spatial variations in water surface area caused by decreasing or increasing water temperature.

In the study, the inversion of Planck function method which is one of the most accurate (RMSE: 2-4 K) Ndossi and Avdan (2016) was used to extract surface temperature from the satellite imageries. The approach starts with defining of the thermal band and the determining of the spectral radiance formatted from (U.S. Geological Survey, 2019) site in order to calculate the brightness temperature, Equation (4.6).

$$L_{TOP} = (M_L * Q_{cal}) + A_L \quad \textbf{(4.6)}$$

Where L_{TOP} = Top of Atmospheric (TOP) spectral radiance value in watts/m²*sr*µm

M_L = band specific multiplication rescaling factor where:

M_L = 0.055375 for Landsat 5, and M_L = 0.0003342 for Landsat 8,

Q_{cal} = quantized and calibrated standard product pixel values

A_L = Resizing factor,

where: A_L = 1.18243 for Landsat 5, and A_L = 0.1 for Landsat 8

Following conversion of reflection values to radiance values, the spectral radiance is converted to a brightness temperature values using formulas provided by (USGS, 2021) utilizing the thermal constants supplied in the thermal band data metadata, Equation (4.7).

$$T_B = \frac{K_2}{ln(\frac{K_1}{(L_{TOP}+1)})} \quad \textbf{(4.7)}$$

Where T_B = The Brightness temperature,

K_1 and K_2 are band-specific thermal conversion constant from the metadata, where:

K_1 = 607.76 and K_2 = 1260.56 for Landsat 5 TM,

K_1 = 774.89 and K_2 =1321.08 for Landsat 8 OLI/TIRS

After that, the normalized differential vegetation index (NDVI) threshold method and the emissivity adjusted lake surface temperature values, which is the effectiveness of thermal energy that is transferred from the surface to the surrounding atmosphere, were obtained to calculate LSWT values (Valor, 1996; Sobrino et al, 2004; Vlassova et al, 2014), Equations (4.8–4.11).

$$LSWT = \frac{T_B}{\{1+\left[\left(\lambda * \frac{T_B}{\alpha}\right) * ln(\varepsilon)\right]\}} \quad \textbf{(4.8)}$$

Where LSWT is Lake Surface Water Temperature,

λ = average wavelength of band,

α = 1.438 * 10^{-2} mK

$$\varepsilon = \begin{cases} 0.985 & \text{for water (NDVI < 0)} \\ \rho_R \text{ (red reflection)} & \text{for bare soil (0 ≤ NDVI ≤ 0.1)} \\ 0.990 * Pv + 0.984 * (1 - Pv) * (0.984 + 0.04 * Pv) & \text{for vegetation mixed with soil (0.1 ≤ NDVI ≤ 0.7)} \\ 0.990 & \text{for vegetation (NDVI > 0.7)} \end{cases} \quad \textbf{(4.9)}$$

ρ_R = reflectance band in the red region of the electromagnetic spectrum

ε = emissivity value is classified according to land cover type based on NDVI values:

$$NDVI = \frac{NIR - Red}{NIR + Red} \quad \textbf{(4.10)}$$

P_v (Akher and Chattopadhyay, 2017) is vegetation proportion and it is calculated using the following equation;

$$P_v = [\frac{(NDVI - NDVImin)}{(NDVImax - NDVImin)}]^2 \quad \textbf{(4.11)}$$

Where NDVI min = 0.2, and
NDVI max = 0.5

In order to evaluate the LSWT results, MODIS LST data were utilized for cross-validation since there is no ground station in the test sites. For the evaluation, the average LSWT time series were compared with MODIS LST, and the correlation results were presented for each lake.

A GEE code was used including the fundamental described equations to calculate the LSWT for each surface lake by applying the suitable metadata values for each Landsat sensor based on its thermal bands as shown below as an example for Landsat 8 sensor.

- Add the NDWI band to the image:

```
var ndwi = img.normalizedDifference(['B3', 'B5']).rename('NDWI').clip(region);
var water01 = ndwi.gt(0);
```

- Calculate water area

```
var without_water = img.updateMask(water01);
var myndwi= water01.updateMask(water01);
var vector = myndwi.reduceToVectors ({geometry: Map.getBounds (true), scale: Map.getScale () * 0.28, maxPixels: 1e12})
```

- Brightness temperature calculations:

```
var calcLSWT = function(img) {
        var BT = img.expression(
            '(k2/log((k1/((M*Tb) +A)) +1)) - 273.15', {
            'Tb': img.select ('B10') })
var toa = img.expression(
        '(0.0003342*Tb) +0.1', {
```

```
                'Tb': img.select('B10') })
  var brightness_temp_semlog = toa.expression(
                                        '(K1 / toa) + 1', {
                                  'K1': 774.8853,
                                        'toa': toa})
   var brightness_temp_log = brightness_temp_semlog.log ()
   var brightness_temp = brightness_temp_log.expression(
                                    '(K2 / brightness_temp_log)-273.15', {
                                      'K2': 1321.0783,
                                      'brightness_temp_log': brightness_temp_log})
```

- NDVI threshold method:

```
  var ndvi = img.expression( '(B5-B4)/(B5+B4)', {
                'B5':img. select('B5'),
                'B4':img. select('B4')})
  var pV = ndvi.expression(
     '(ndvi - ndvi_min) / (ndvi_max - ndvi_min)',
  'ndvi_max': 0.5,
  'ndvi_min': 0.2,
  var pV_pow = pV.pow(2);
  var lse = pV_pow.expression(
          '(0.04 * pV) + 0.984', {'pV': pV_pow})
  var lse_log = lse.log ()
```

- LSWT determination

```
  var lswt = brightness_temp.expression
              'BT / (1 + (11.5 * BT / p) * lse_log)', {
                          'p': 14380, 'BT': brightness_temp,
                          'lse_log': lse_log })
  var LSWT = img.addBands(lswt)
  return LSWT};
  var LSWT = l8images.map(calcLSWT)
```

4.4 Relationship Between Lake Surface Extent and LSWT Variables

The previous sections describe how the GEE platform was used to calculate surface water extent and LSWT variables for the three lakes from 2000 to 2021. In this section, the LSWT time series is displayed on the water surface area time series as a

supplementary y-axis through charts in Excel, which will present in the next chapter, to explore potential connections between lake water extents and the LSWT variable.

5. ANALYSIS AND RESULTS

5.1 Accuracy Assessment of Extracted NDWI Maps

The extracted findings from the Landsat images clipped to each lake border were compared point-to-point with the NDWI map for the minimum and maximum water surface area values to demonstrate the accuracies of our results across the research period (2000-2021). Table 5.1 displays the smallest and largest lake area values, as well as their accuracy for Users, Producers, and Overall.

Table 5.1 : The accuracy assessment of extracted water pixels with NDWI.

	Burdur Lake Oct 10, 2021 Landsat 8	Burdur Lake May 20, 2004 Landsat 5	Egirdir Lake Oct 10, 2021 Landsat 8	Egirdir Lake Mar 17, 2004 Landsat 5	Beysehir Lake Sep 17, 2001 Landsat 5	Beysehir Lake Apr 27, 2013 Landsat 8
	Smallest area	Largest area	Smallest area	Largest area	Smallest area	Largest area
Area (km^2)	120.53	159.29	439.85	467	605.89	685.01
User Accuracy % (Water)	99%	99.1%	98.3%	98%	100%	97.7%
Producer Accuracy % (Water)	100%	100%	100%	100%	99%	100%
Overall Accuracy %	99.3%	99.45%	98.7%	98.5%	99.3%	98.7%
Kappa	0.983	0.988	0.959	0.963	0.984	0.973

After generating the confusion matrix for maximum and minimum water surface area in each lake during a 21-year period, Overall accuracy of the results was more than 98%, as the accuracy of the Producer and User for water areas was more than 97%. Moreover, Kappa coefficient values are close to 1, representing perfect agreement. For the suggested extraction techniques outcomes in this study, the assessment demonstrates an accuracy with a high degree in water extraction, which is indicative of its effectiveness and simplicity; it also demonstrates that this approach can be used in other relevant geographic regions for future research.

5.2 Spatio-temporal Changes in Lake Water Extent

The water surface area for each lake during the study period (2000-2021) was calculated. Thus, the daily, seasonal, and annual spatio-temporal changes in area were determined and presented via charts through Microsoft Excel. The changes have been calculated after analyzing the collected Landsat images (606 images) in GEE cloud platform, which was used to employ the NDWI in order to calculate the water surface area from each filtered image.

5.2.1 Lake Burdur

Burdur Lake's water surface area, which was 180 km² in 1990 (General Directorate of Water Management, 2015), it was assessed to be 156 km² in the summer of 2000, as shown in Figure 5.1. The value of surface water area, which was 158 km² in the first four months of 2000, decreased to 156 km² throughout the summer and to 154 km² at the conclusion of the year. In the winter of 2001, the extent of the lake's surface was 155 km²; however, throughout the summer, it decreased to 153 km², and then reduced to 151 km² by late fall of 2001. The water surface area value of 152 km² in the start of 2002 fluctuated somewhat and settled at 151 km² by the conclusion of the year. However, in the summer of 2003, the area value was raised from 151 km² to 154 km² then returned to 152 km² at the end of the autumn. At first of 2004, the surface water area value was 156 km² it was increased when we compared it with the previous year value and the value kept increasing throughout the summer also 157 km² until the autumn season, it was 155 km². There was no significant change in the value of the lake area during the year 2005, as the decreasing change ranged from 155 km² in the first few months of the year to 153 km² at the end of the year. The water surface area, which was 153 km² in the winter of 2006, decreased to 151 km² in the autumn of the same year. In the spring of 2007, the surface area was 150 km², but by the end of the year it had dropped to 147 km². The decrease in the area of the lake continued in 2008, when the area was 145 km² in the summer of the year and became 143 km² at the autumn. The lake surface area was 144 km² in the spring of 2009 and it dropped to 141 km² by the end of the year. In the summer of 2010, the lake surface extent was 143 km², but it decreased to 140 km² by the conclusion of the year. As of the end of 2011, the area value was 139 km², down

from 142 km² at the beginning of the year. For 2012, there were no images, and so no area values.

During the spring season of 2013, the lake's water surface area decreased to 138 km², then recovered to 135 km² before the end of the same year. The water surface area which was 135 km² at the start of 2014, decreased by 132 km² by the conclusion of the year. In 2015, the water surface area was 137 km² in the spring, and it is dropped to 136 km² in the summer season, then decreased again to 134 km² by the last few months of the year. Whereas the lake's surface area value was 133 km² at the start of 2016 fluctuated somewhat during the year, it gradually decreased to 130 km². It was 130 km² at the start of 2017, fluctuated similarly to 2016 and fell to 127 km² at the year's end. Similarly, the lake's surface area did not change much in 2018, with 127 km² at the start of the year and 126 km² at the end of the year. It decreased from 125 km² in the summer of 2019 to 124 km² in autumn of the same year. The lake's surface area dropped from 124 km² at the start of the year to 122 km² at the year's end in 2020. It has shrunk from 122 km² in the spring of 2021 to 120 km² by December.

The lake surface area trend and the temporal changes between 2000 and 2021 are shown in Figure 5.1. There is no doubt that throughout the course of the last two decades, the area of the lake has steadily dropped over the last 21 years, except for the period from 2003 to 2004, where the surface water area's decline ceased and began to recover. It rose slightly from 154 km² in 2003 to 157 km² in 2004. After 2004, the area continued to decrease at a steady rate, and the annual area trend has been decreasing at the same rate until 2021. Between 2000 and 2021, the area value of the lake that achieved its highest values in the 2003-2004 period, decreased by more than 22%, from an average area of 156 km² in 2000 to 121 km² in 2021.

Figure 5.2 illustrates the seasonal lake area changes between 2000 and 2021, It indicates that the lake's water surface area was reduced in the summer and autumn seasons but increased during the winter and spring seasons. These findings demonstrate a substantial correlation between the water surface area of the lake and the rainy season. Figure 5.3, shows the areal changes in water surface area of five different years, 2000, 2005, 2010, 2015, and 2021. Consequently, the changes of Burdur Lake surface extent were calculated, taking into account such periods as 158, 155, 142, 135, and 121 km², respectively.

The annual variations were calculated based on the 2000 and are shown in Figure 5.4. Generally, except for the year 2004, when the lake's surface area achieved its highest values and recovered by 0.7% with respect to the water surface area in 2000, the lake surface area decreased most of the time. The worst redaction occurred in 2021, when the lake's surface area decreased by 22.21%. If the lake's circumstances continue to deteriorate, the lake's area will shrink by half in six years.

The primary causes of such a massive change would be the impacts of climate change on the basin and the exaggerated use of water sources that were meant to feed the lake as the lake is close to the city center (Firatli et al., 2022). Lake Burdur, located in a closed basin, is fed by precipitation, water flowing into the lake from rivers/streams and groundwater. Over the years, dams and ponds were erected on streams/rivers that deliver water to Lake Burdur, thus the only water source of the lake is precipitation. As a result, after the construction of the dams and ponds over the rivers/streams that are the main sources feeding the lake, the water level of the lake decreased fast due to low precipitation and high evaporation rates.

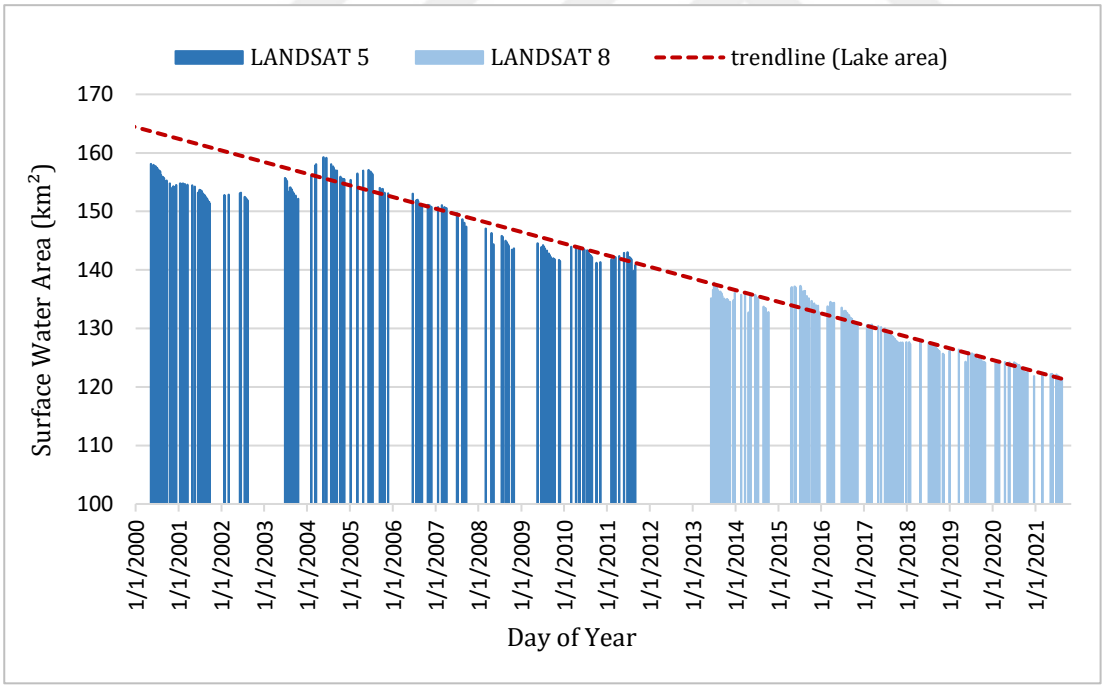

Figure 5.1 : Temporal changes of water surface extent and its trendline for Lake Burdur between 2000 and 2021.

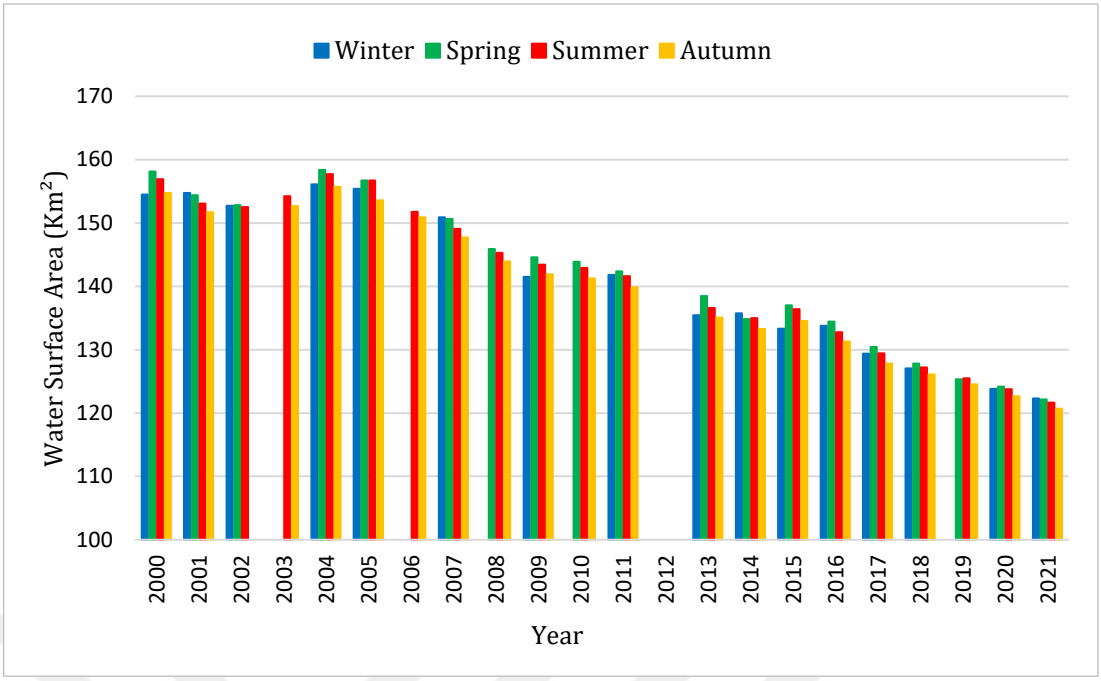

Figure 5.2 : Seasonal water surface extent changes in Lake Burdur.

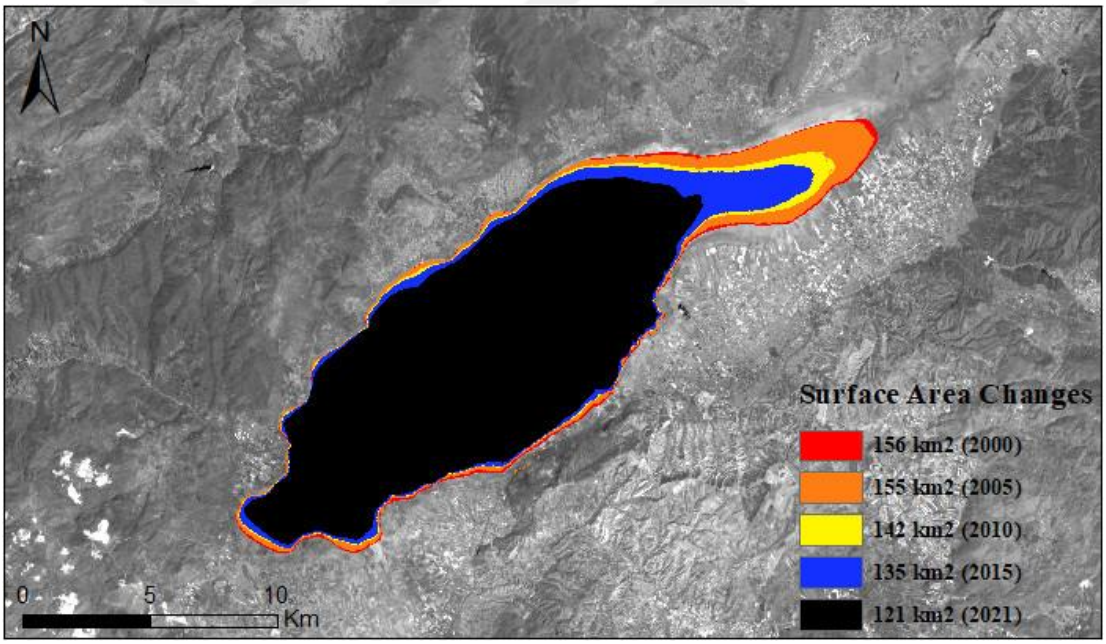

Figure 5.3 : Spatial changes in water surface area according to years for Lake Burdur.

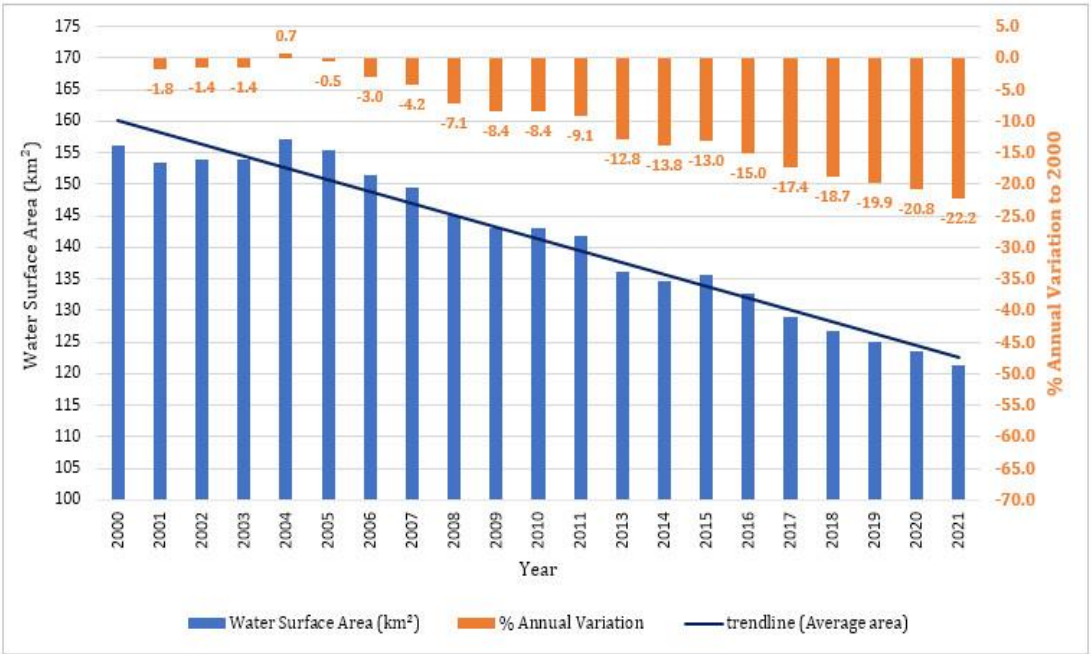

Figure 5.4 : Long-term annual water surface area variations of Burdur Lake.

5.2.2 Lake Egirdir

The Egirdir Lake has freshwater and it is located in the Isparta region that was created by tectonic and karstic forces. Along with serving as a drinking water basin, it is significant waterbody for its biological benefits and irrigation uses. In the study period for Egirdir Lake, the lake surface area was 461 km² in the winter of 2000 and decreased in the autumn of the same year to be 458 km² as shown in Figure 5.5, which presents a time series for the surface water extent changes. In the spring of 2001, the area, which was 458 km², decreased to 453 km² in December of the same year. In the spring of 2002, the water surface area was estimated at 463 km², while by the summer, it had dropped to 454 km². Until the summer of 2003, there was no imagery accessible, thus the lake surface area was determined to be 455 km² in that season and it was with the same extent till the year's end. The lake surface area was 455 km² in the summer of 2004, while it increased to 458 km² in the autumn, and it was at the same rate in 2005. There was no imagery in any season of 2006 except the summer when the water surface area was 454 km². The water surface extent was 461 km² in the winter of 2007 and it decreased to be 453 km² in the autumn. In the summer of 2008, the surface area was 452 km² and it decreased to 451 km² in the autumn. The lake's surface extent was assessed to be 453 km² in the spring season of 2009, and it dropped to 452 km² throughout the summer, before increasing to 453 km² towards year's end. In the spring of 2010, the lake surface area was 457 km² then it dropped to 453 km² in the summer

of the same year. At the start of 2011, the surface area value of Lake Egirdir was 453 km², after that it decreased to 453 km² in the summer, and kept with the same value until the conclusion of the year. During 2012, there were no images, hence no surface water area values.

Although there were no images during some of the years' winters, the area value for the winter of 2013 was 462 km², which was reduced to 454 km² in the year's end. The surface area was 454 km² in the summer of 2014 and then it dropped to 453 km² in the autumn. In the first months of 2015, the water surface area was 461 km², then reduced to 454 km² in the summer, while increased to 460 km² by the year's end. It was assessed to be 461 km² in the spring of 2016, but by the summer it had dropped to 454 km² and stayed thus until the autumn. The lake's surface area was first estimated at 457 km² in the spring of 2017 before being decreased to 453 km² in the autumn of the same year. The summer of 2018 saw the area decrease from 460 km² to 451 km² from the winter of 2018. In 2019, the lake surface area was 453 km² through the spring season, and it decreased to 450 km² in the last of the year. There was a noticeable change in the surface area of the lake in 2020, as the area was 457 km² at the first of the year and decreased to 446 km² by the year's end, decreasing by more than 10 km². While, the lake surface area was 448 km² in the spring of 2021, and it dropped to 440 km² in the autumn of the same year.

During the first few months of 2004, the lake's water surface area reached its peak, topping 467 km², and it reached its lowest area value of 440 km² in the autumn of 2021, as shown in Figure 5.4. The water surface area of the lake, which was at its maximum in 2004, decreased by more than 3% (15 km²), from an average area of 458 km² in 2000 to 443 km² in 2021.

The lake's surface area increased in the winter and spring seasons and decreased in the summer and autumn, indicating a seasonal fluctuation in the lake's extent as can be seen in Figure 5.6, thus it is presenting the seasonal changes in water surface area. An empty bar means there is no data or cloud-free image for the given season in that year. These findings demonstrate a close relationship between the lake surface area and the rainy season. In addition, during the summer months, irrigation water often decreases (Avraz et al, 2014). Figure 5.7, shows the areal changes in water surface area of five different years, 2000, 2005, 2010, 2015, and 2021. Consequently,

the changes of Egirdir Lake surface extent were calculated, taking into account such periods as 458, 457, 454, 456, and 443 km², respectively.

The variance in Egirdir Lake extent is just 5–15 km² during the study period, which is only 3–4% of the year 2000 surface water area, as seen in Figure 5.8, which shows the annual variations in lake water surface extent compared with respect to the water surface area in 2000. The highest rate of surface water recovery occurred in 2004, when it increased by 0.05% over the annual average for the year 2000. While, the worst redaction within the study duration occurred in 2021, when the lake's surface area decreased by 3.39%.

When comparing Burdur and Egirdir Lakes, the size of Lake Egirdir was almost three times more than Lake Burdur in 2000, and it is not close to the city center as Lake Burdur. Besides, the number of constructed ponds and dams over the rivers/streams feeding the lake are not as many as Lake Burdur. These circumstances may have contributed to the surface water area of Lake Egirdir by being less impacted by human activities than Lake Burdur.

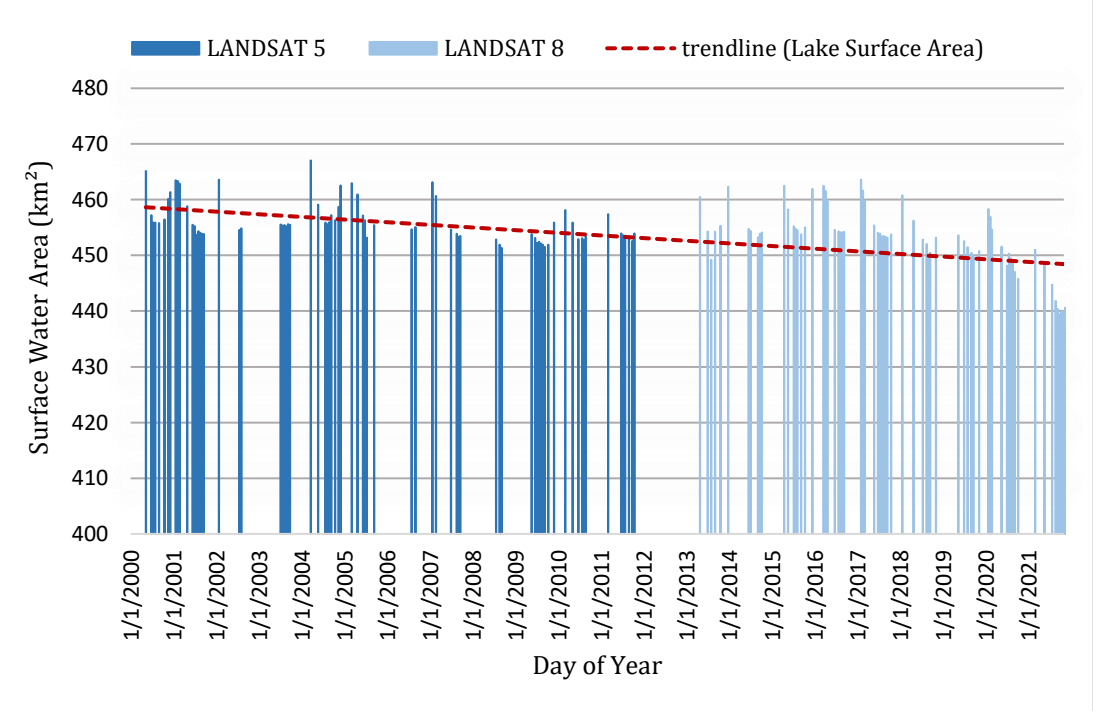

Figure 5.5 : Temporal changes of water surface extent and its trendline for Lake Egirdir between 2000 and 2021.

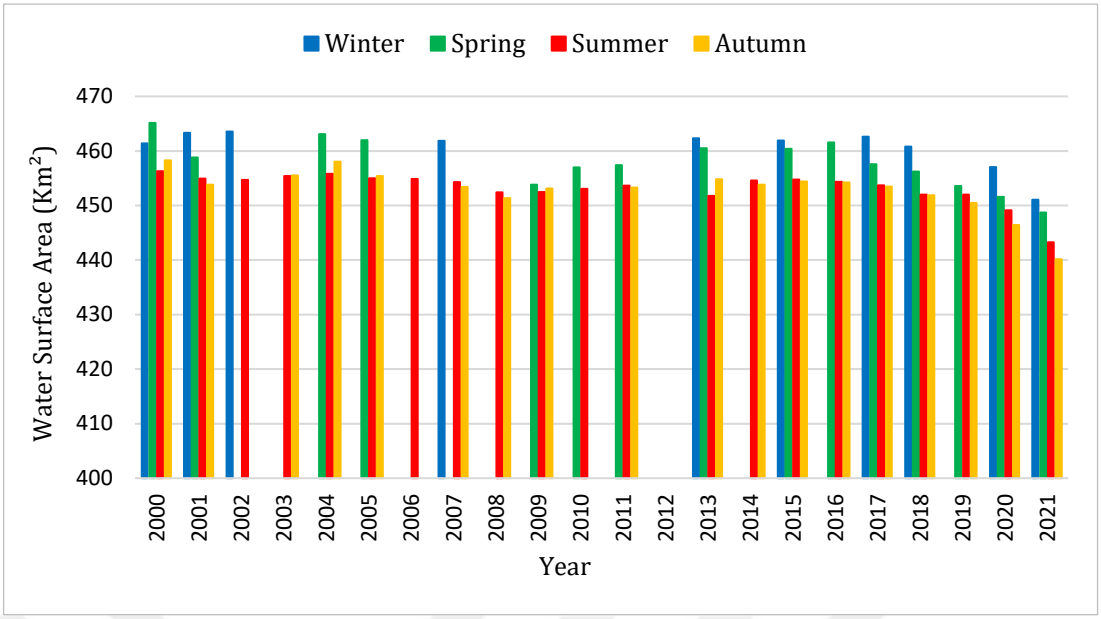

Figure 5.6 : The seasonal water surface extent changes of Lake Egirdir.

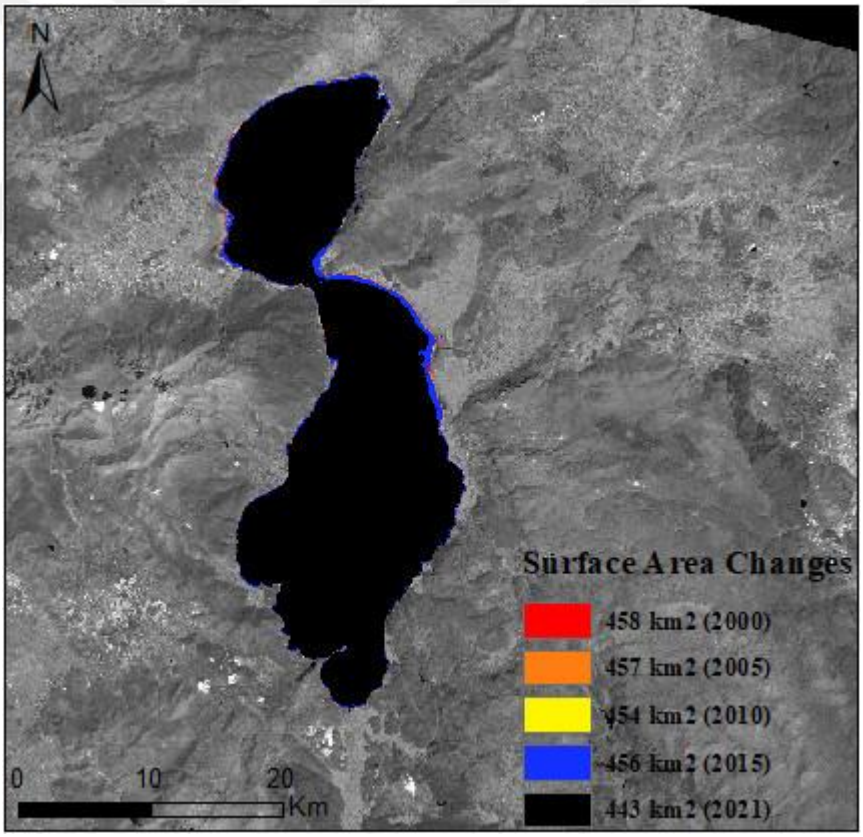

Figure 5.7 : Spatial changes in water surface area according to years for Lake Egirdir.

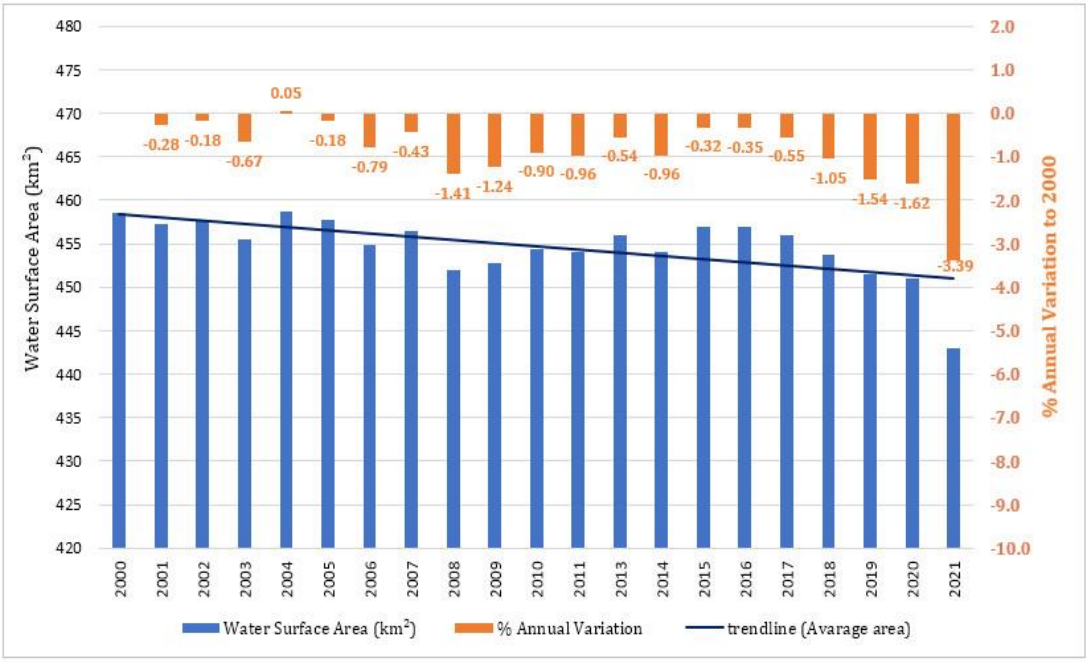

Figure 5.8 : Long-term annual water surface area variations of Egirdir Lake.

5.2.3 Lake Beysehir

In Beysehir Lake, after analyzing the remote sensing images, there hasn't been much of a change in the water surface area. During the study period between the years 2000 to 2021, the average annual area trended to increase slightly, as seen in Figure 5.9. In the 2000 spring season, the surface water area of Beysehir Lake decreased from 635 km² to 622 km² in autumn. In the winter of 2001, the lake surface area was 627 km², it decreased to 615 km² in the summer and dropped to 606 km² in the autumn of the same year. Beysehir Lake seldom receives satellite images in the winter season, thus their surface area increased in the spring season and decreased in autumn, indicating seasonal variation, but with a general trend toward decline until the end of 2001. In comparison to the previous year (2001), the lake's surface extent increased from 612 km² in the spring of 2002 to 625 km² in summer. It was assessed to be 625 km² in summer and 623 km² in the autumn of 2003, with no significant change. The lake surface area changes through spring to autumn in 2004 was 645 km² and 625 km², while the extent that changed from spring to autumn in 2005 was 634 km² and 611 km². In 2006, the surface area was 613 km² in summer, while there were no images in the rest of the seasons. At the beginning of 2007, the lake surface area was calculated to be 632 km², then decreased to 619 km² in summer and 616 km² in autumn of the same year. Summer and autumn variations of water surface area were determined at 616 km² and 611 km² in 2008, and 625 km² and 623 km² in 2009, respectively.

In the spring of 2010, the extent of the lake increased compared with its value in the previous year (2009). It was 648 km² and decreased to 626 km² in the summer. In the spring of 2011, it was first estimated at 641 km² before being decreased to 630 km² in autumn.

In Beysehir Lake, which does not have any imagery from 2012, an area of 685 km² has been determined, with the maximum value occurring in the spring of 2013 and a subsequent reduction to 637 km² occurred in the autumn of the same year. A lot of the single images were not included in our evaluation, because they couldn't cover the whole lake due to the huge lake surface area, so in the spring season of 2013, just one single Landsat image was recorded, which then gave the maximum lake area. There was no imagery in the spring season of 2014, and the water surface area was 635 km² in summer, then it dropped to 631 km² in autumn. In 2015, through the spring season, the lake surface extent was 657 km², while it decreased to 636 km² by the year's end. The change of lake surface area through spring to autumn was detected to be 652 km² and 621 km² in 2016, and 647 km² and 630 km² in 2017. The winter of 2018 showed an increase of 651 km² in Beysehir's Lake surface area compared to 2017. However, in summer and autumn, the surface area value decreased to 626 km². There was another reduction in the area value from 633 km² in the spring of 2019 to 627 km² in the autumn season of 2019. At the start of 2020, the lake surface area was 657 km². Then it was determined to be 639 km² in the spring season and it has been declining to reach 627 km² in autumn of the same year. According to analyzed imagery from spring 2021, the lake's extent was 637 km² and then reduced to 618 km² in autumn of the same year.

An area of 685 km² has been determined, with the maximum value occurring in the spring of 2013, which is the year that has experienced the most significant increase throughout the study duration. This increase was due to an increase in the amount of precipitation that year. Despite the slight increase in the direction of water surface extent during the 21-year period, the average water surface area, which was 627 km² in 2000, decreased to 623 km² in 2021 (Figure 5.9).

In contrast to the summer and autumn seasons, the lake's area values increased to their highest levels ever recorded in the winter and spring seasons, as seen in Figure 5.10, which shows the seasonal changes in lake surface extent during a 21-year period. The appearance of an empty column implies that no data is available for that season. There have been a few modest changes within the spring and autumn seasons. Spring

readings have generally been somewhat greater than autumn ones. This was because of irrigation water use in Beysehir Lake's region. Figure 5.11, shows the areal changes in water surface area of five different years, 2000, 2005, 2010, 2015, and 2021. Consequently, the changes of the Lake surface extent were calculated, taking into account such periods as 627, 622, 633, 442, and 623 km²

Generally, reductions in lake area occurred most frequently before 2013, as seen in Figure 5.12, which shows the percentage of annual variation for water surface area in comparison to lake surface area values of 2000. The worst redaction within the study duration occurred in 2001, when the lake's surface area was decreased by 2.25% with the minimum water surface area value of 606 km², which was recorded in the autumn season. Even though the lake's surface water area had the highest rate of recovery in 2013, it went up by 3.18% with annual variation.

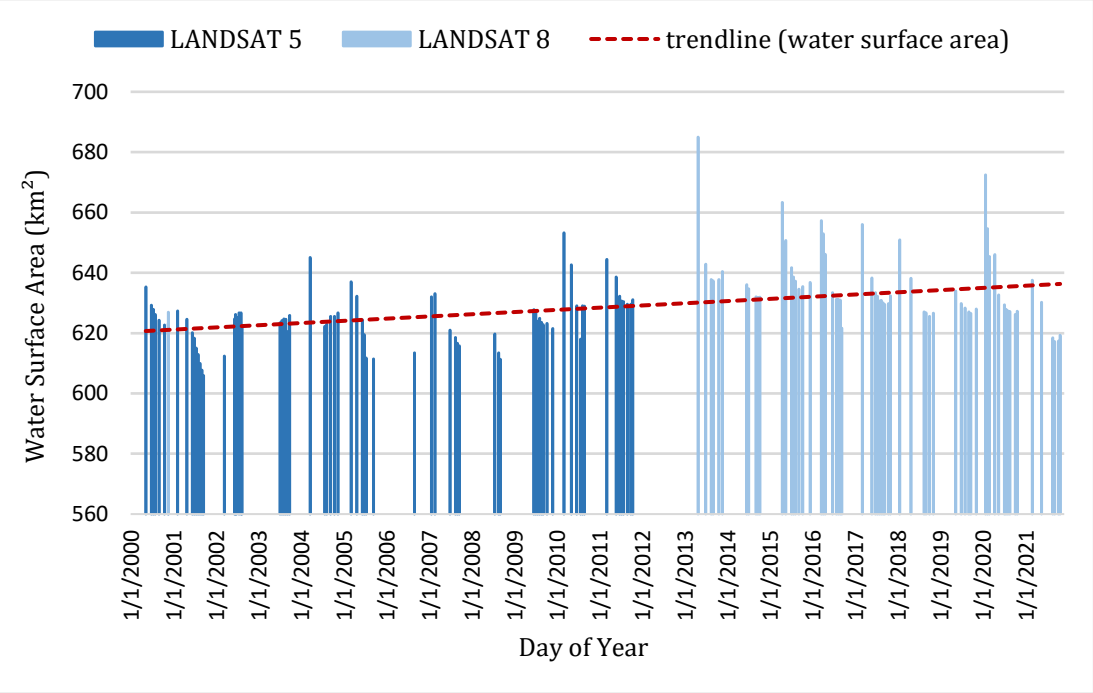

Figure 5.9 : Temporal changes of water surface extent and its trendline for Lake Beysehir between 2000 and 2021.

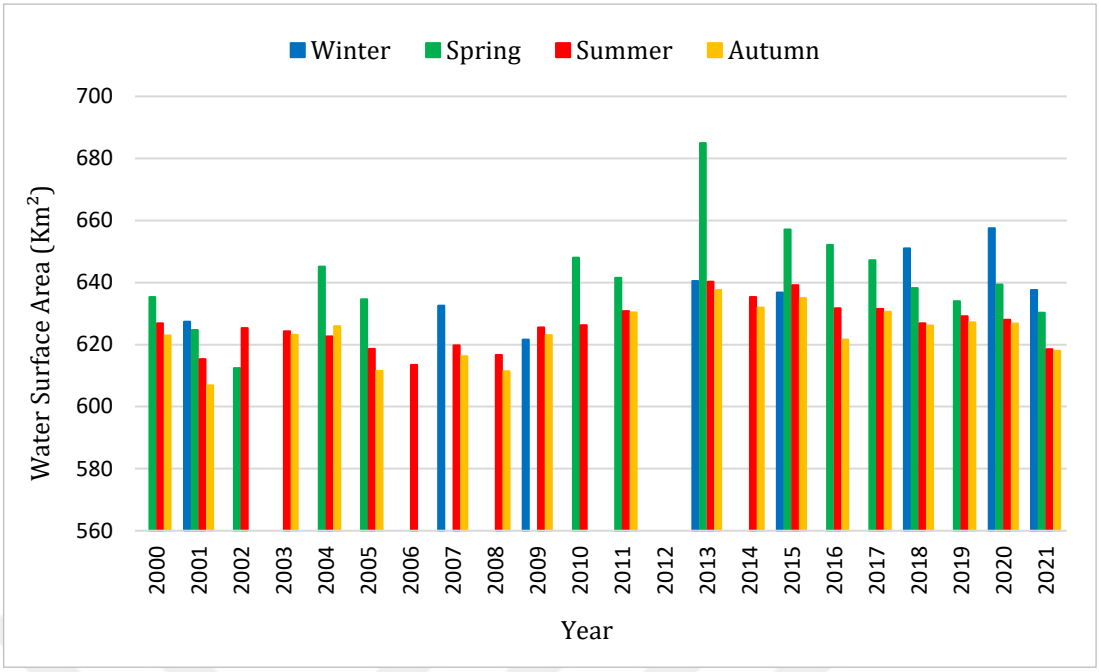

Figure 5.10 : The seasonal water surface extent changes of Lake Beysehir

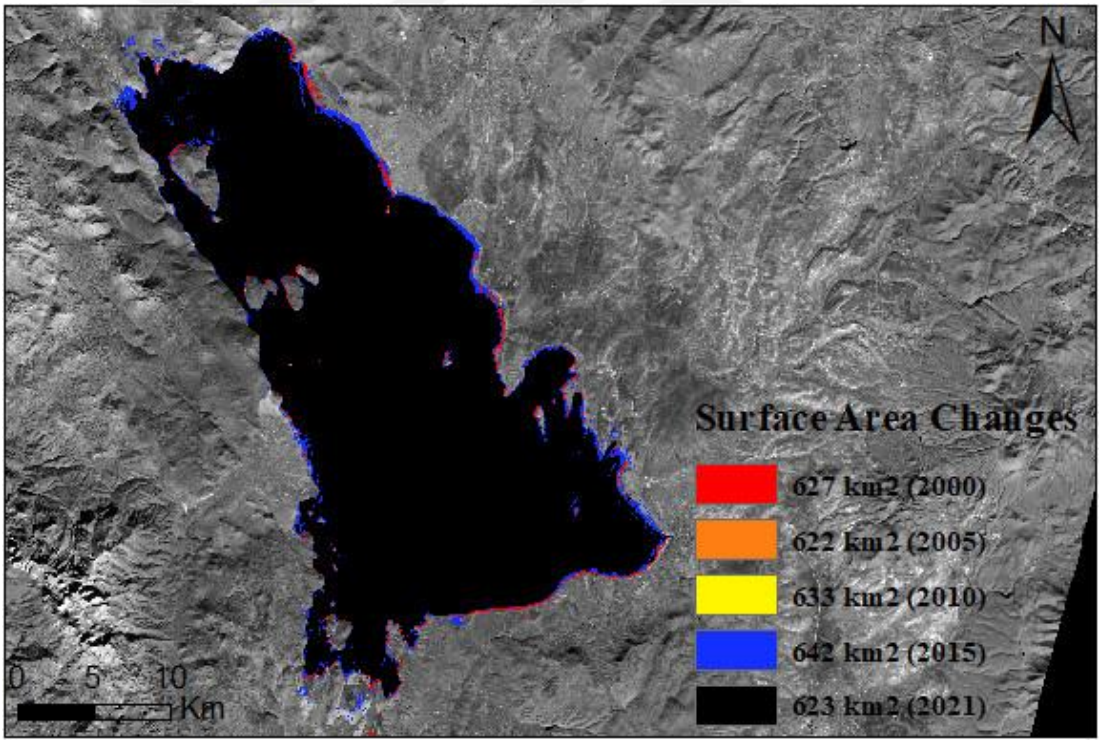

Figure 5.11 : Spatial changes in water surface area according to years for Lake Beysehir.

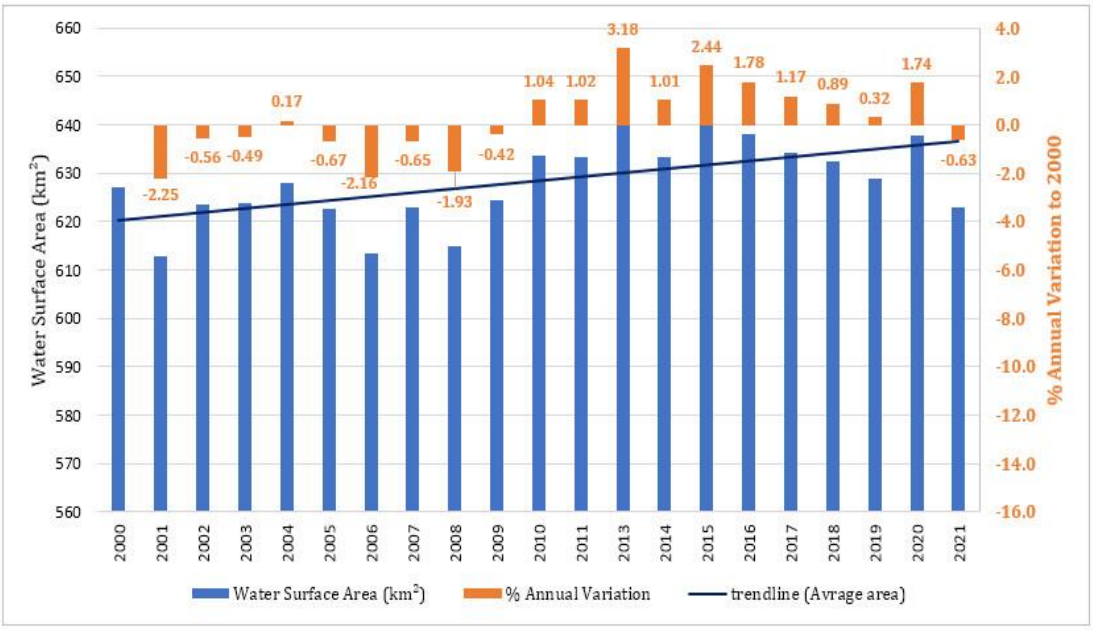

Figure 5.12 : Long-term annual water surface area variations of Beysehir Lake.

In summary, Table 4.1 displays the highest and lowest lake surface area values in the three lakes between 2000 and 2021 along with the corresponding year. The table shows the lake surface area value for the reference time period. For example, the maximum water surface area of Lake Burdur was 159 km², reached in the spring of 2004, and the lowest value of 120.7 km² which was in the spring of 2021. Additionally, Table 5.2 displays the average water surface area value for 2021, as well as it gives the percentage of the recent area value in 2021 with relative to the maximum one. This shows the proportion of the lake's surface area compared to its greatest extent.

Table 5.2 : Lakes' maximum and minimum surface water area values as well as their recurrence dates.

Lake	Maximum area value (km²)	Date of Maximum area value	Minimum area value (km²)	Date of Minimum area value	Area value in 2021 (km²)	% Of area value in 2021 compared to maximum value
Burdur	159	2004	120.7	2021	121.4	76.4%
Egirdir	467	2004	440.1	2021	442.9	94.8%
Beysehir	685	2013	606.8	2001	623	90.9%

5.3 Relationship Between LSWT and Lake Water Extent Changes

The lake surface water temperature for the three lakes was examined, and an increasing trend was observed for all of them, since the annual average value of Lake Burdur was 19.01° C in 2000 and it increased to 22.91°C in 2021, increasing by 2.13°C, while it was 15.86°C in 2000 and 16.18°C in 2021 for Lake Egirdir, increasing by more than 0.3°C, and for Lake Beysehir, the value, which was 17.03°C in 2000, decreased to 15.54°C in 2021, decreasing by less than 1.5°C as seen in Figure 5.13, which shows the annual mean of LSWT during the study duration. No images were available for the year 2012. As a result, the year's average water temperature value is not computed.

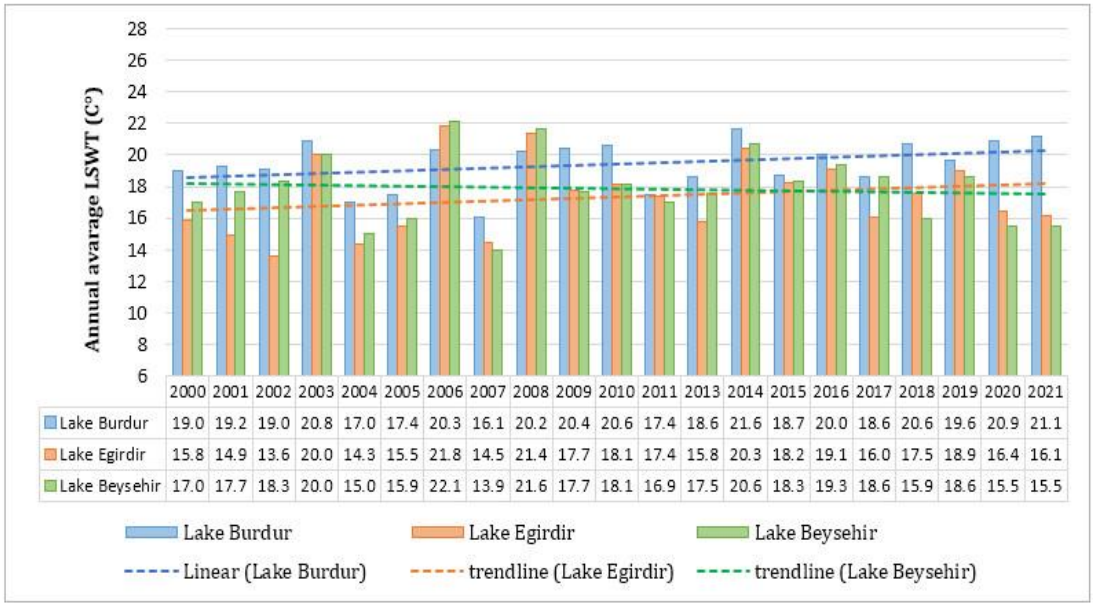

	2000	2001	2002	2003	2004	2005	2006	2007	2008	2009	2010	2011	2013	2014	2015	2016	2017	2018	2019	2020	2021
Lake Burdur	19.0	19.2	19.0	20.8	17.0	17.4	20.3	16.1	20.2	20.4	20.6	17.4	18.6	21.6	18.7	20.0	18.6	20.6	19.6	20.9	21.1
Lake Egirdir	15.8	14.9	13.6	20.0	14.3	15.5	21.8	14.5	21.4	17.7	18.1	17.4	15.8	20.3	18.2	19.1	16.0	17.5	18.9	16.4	16.1
Lake Beysehir	17.0	17.7	18.3	20.0	15.0	15.9	22.1	13.9	21.6	17.7	18.1	16.9	17.5	20.6	18.3	19.3	18.6	15.9	18.6	15.5	15.5

Figure 5.13 : The long-term annual average LSWT for the three lakes.

5.3.1 LSWT of Lake Burdur

In 1998, based on Aslan and Koc-San (2021), Burdur Lake's surface area was roughly 161 km², but by 2018, it had shrunk by 127 km². Thus, it has lost in a percentage with more than 20% of its surface area in the last two decades, while the LSWT value increased by 2.2° C throughout the same time period. According to our research, after analyzing the data, the surface water temperature in Burdur Lake has risen, and the trend is upward. In the study period from 2000 to 2021, the lake surface area decreased by 35 km², while LSWT increased by more than 2.1°C, as seen in Figure 5.11, which shows the changes in the lake surface extent with LSWT.

The average values of LSWT for the summer and autumn seasons in years 2000 and 2021 have been evaluated and extracted according to the NDWI map of year 2000 to show the spatial changes that occurred in water surface area due to a decrease or increase in water temperature. The LSWT values varied between 20.4°C and 35.7°C in the summer of 2000, while the temperature increased in the summer of 2021 to between 22.4°C and 35.9°C, as seen in Figures (5.14a and c), which show the LSWT maps for the summer seasons of years 2000 and 2021, respectively. In the autumn season, the LSWT values, which varied between 11.3°C and 20.5°C in 2000, increased in the same season of 2021 to be between 15.5°C and 24.1°C, as seen in Figures (5.14 b and d). More than 22 % of the lake surface area has been lost during the previous 21 years. This shows that the temperature of the surface water and the extent of the lake's surface are directly related.

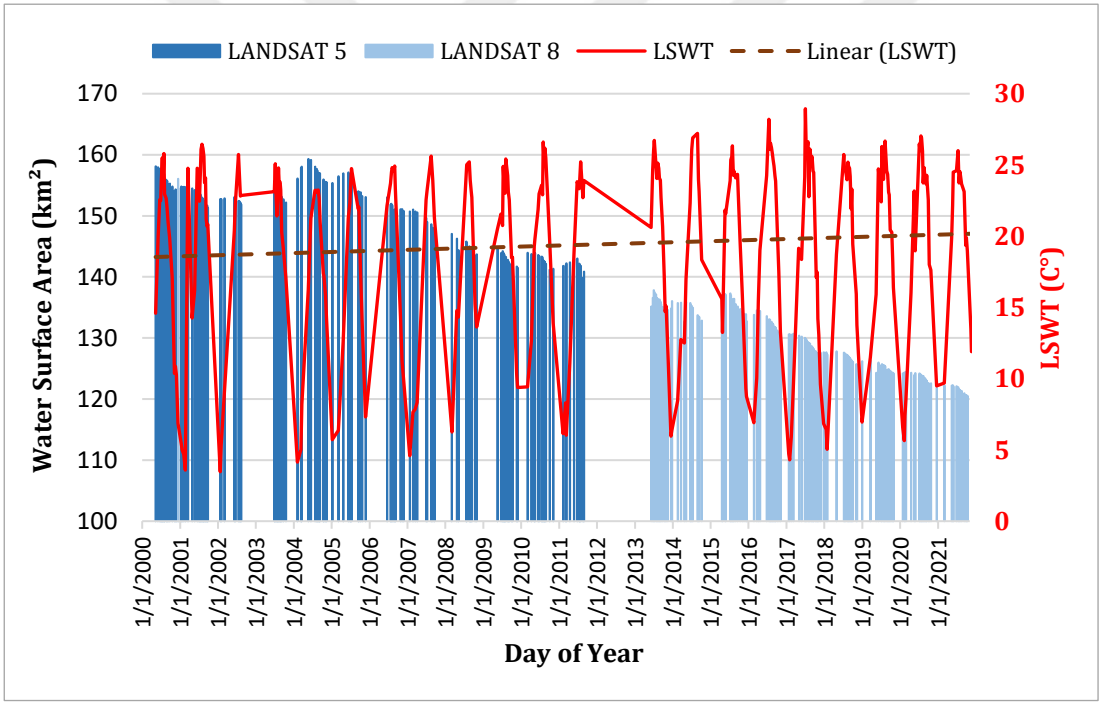

Figure 5.14 : The temporal changes in surface extent of Burdur Lake with the LSWT variable.

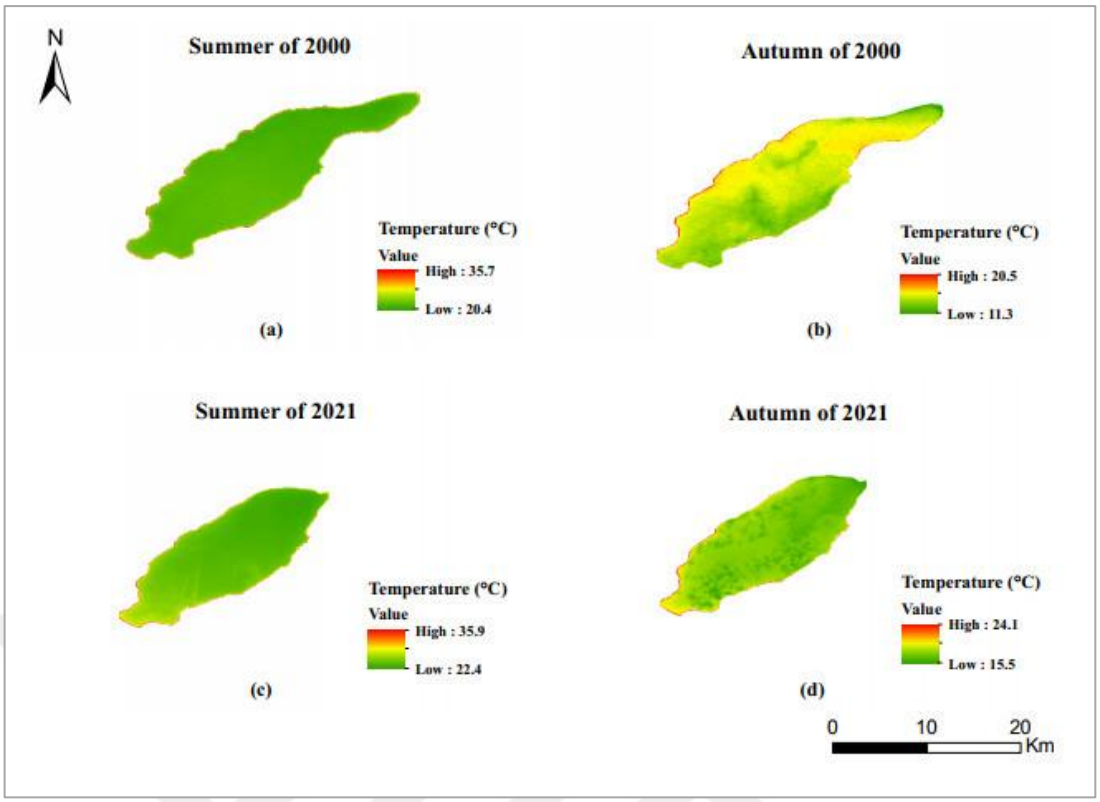

Figure 5.15 : The spatial changes of Burdur Lake's surface area with LSWT for: (a) summer 2000, (b) autumn 2000, (c) summer 2021, and (d) autumn 2021.

5.3.2 LSWT of Lake Egirdir

Based on Aslan and Koc-San (2021), the connection between the lake surface extent and the change in LSWT had been analyzed. It was found that the values of LSWT increase as the lake extent decreases. Between 1998 and 2018, the LSWT values of Egirdir Lake increased by more than 1.3°C and the lake's surface area shrank by less than 4 km².

According to the determined data in our study, the surface water temperature in Egirdir Lake has increased by more than 0.3°C, while the water surface area has decreased by 15 km² through the study period from 2000 to 2021, as seen in Figure 5.15, which shows the changes in lake surface extent with the LSWT variable. As can be noticed from Figure 5.15, the highest decrease of the lake water surface area occurred in 2021, this explains the difference in the decline if compared with Aslan's study.

The average values of LSWT for the summer and autumn seasons in the years 2000 and 2021 have been calculated to show the spatial changes that occurred in the water surface area due to a decrease or increase in water temperature. The LSWT values varied between 17.5°C and 34.8°C in the summer of 2000, while the temperature

values increased in the summer of 2021 to be between 20.9°C and 39°C, as seen in Figures (5.16a and c). In the autumn season, the LSWT values, which varied between 7.9°C and 24.1°C in 2000, increased in the same season of 2021 to be between 9.8°C and 22.7°C as seen in Figures (5.16b and d). The lake has lost less than 3% of its surface area during the 21-year period, indicating that water temperature has had an impact on the lake's extent.

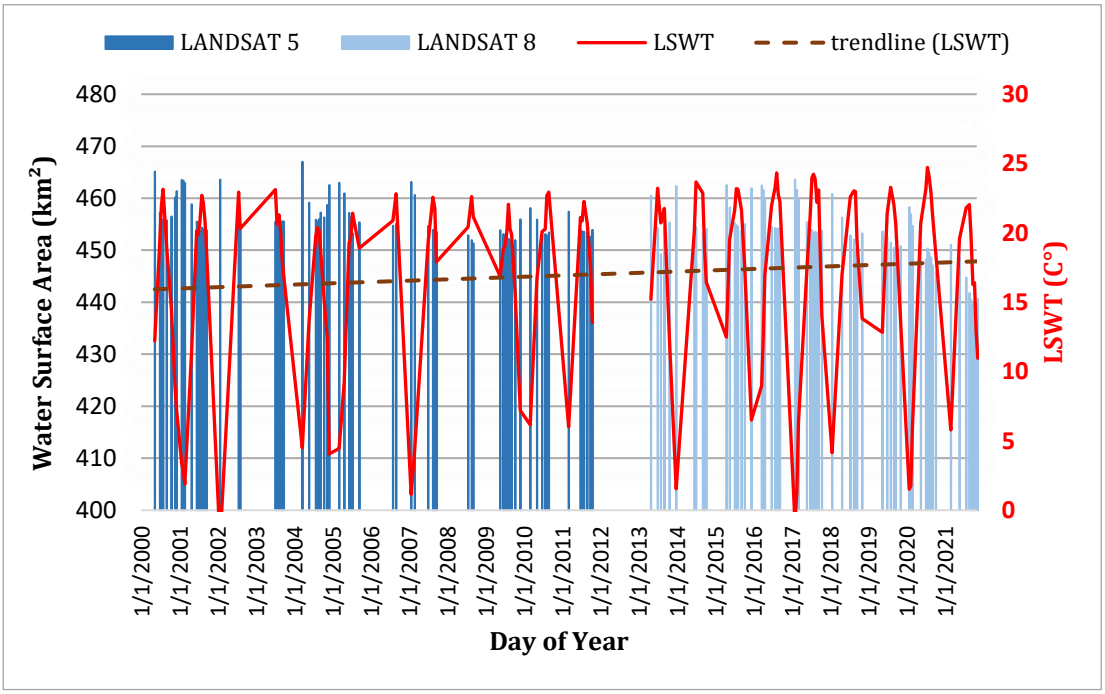

Figure 5.16 : The temporal changes in surface extent of Egirdir Lake with the LSWT variable.

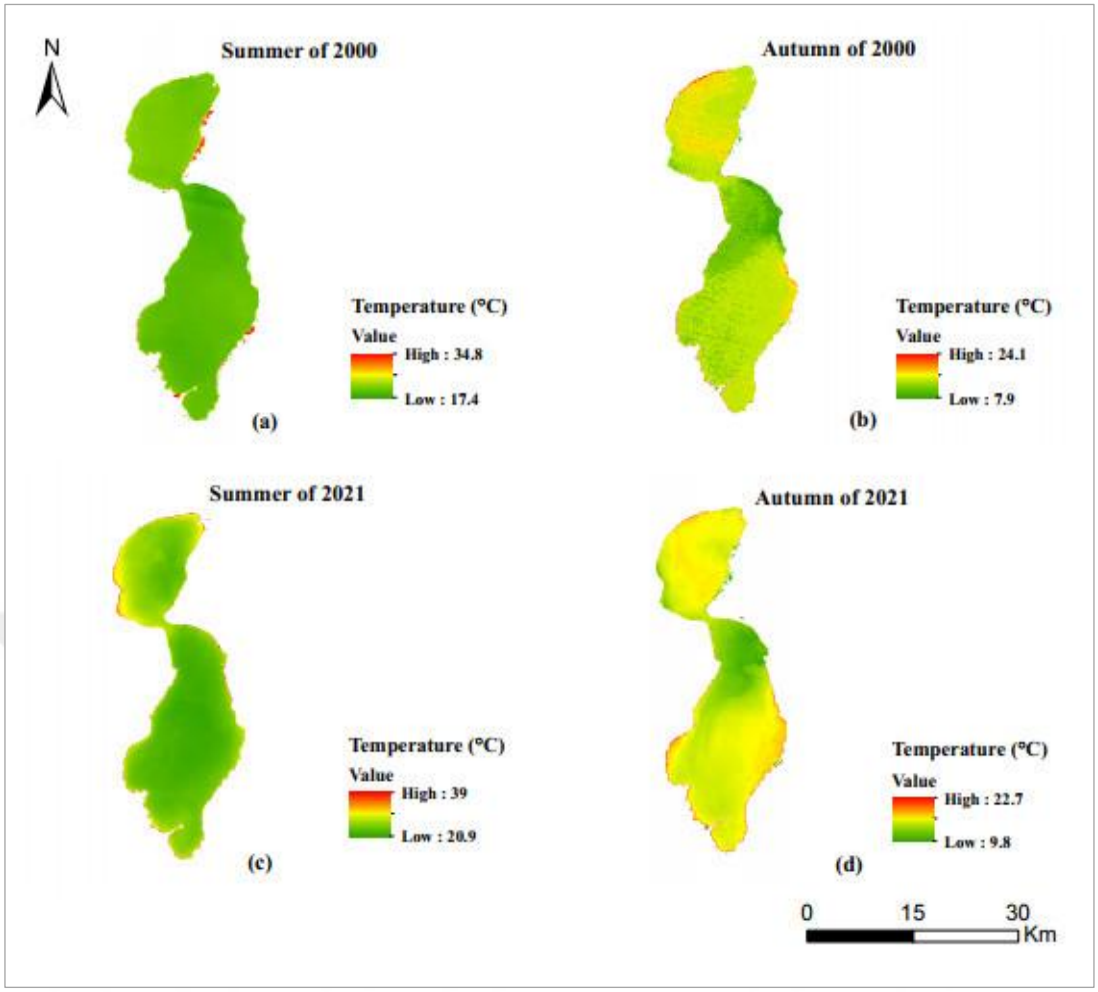

Figure 5.17 : The spatial changes of Egirdir Lake's surface area with LSWT for: (a) summer 2000, (b) autumn 2000, (c) summer 2021, and (d) autumn 2021.

5.3.3 LSWT of Lake Beysehir

According to the data that has been analyzed for Lake Beysehir, the lake's water surface temperature tendency has decreased very slightly. As seen in Figure 5.18, which depicts the decrease in the daily LSWT by more than 1.4°C, while the water surface area decreased by less than 4 km² throughout the end of the study period.

The spatial changes in Beysehir Lake's surface area with the average of LSWT for the summer and autumn seasons in 2000 and 2021 have been extracted. The LSWT values varied between 20.6°C and 39.9°C in the summer of 2000, while the temperature values decreased in the summer of 2021 to be between 21.3°C and 31.9°C, as shown in Figures (5.19a and c). In the autumn season, it has risen from a range of (11.9 – 26.7) °C in 2000 to (15.4 – 35.3) °C in 2021.This explains the slight decrease in the lake surface area by roughly 1%.

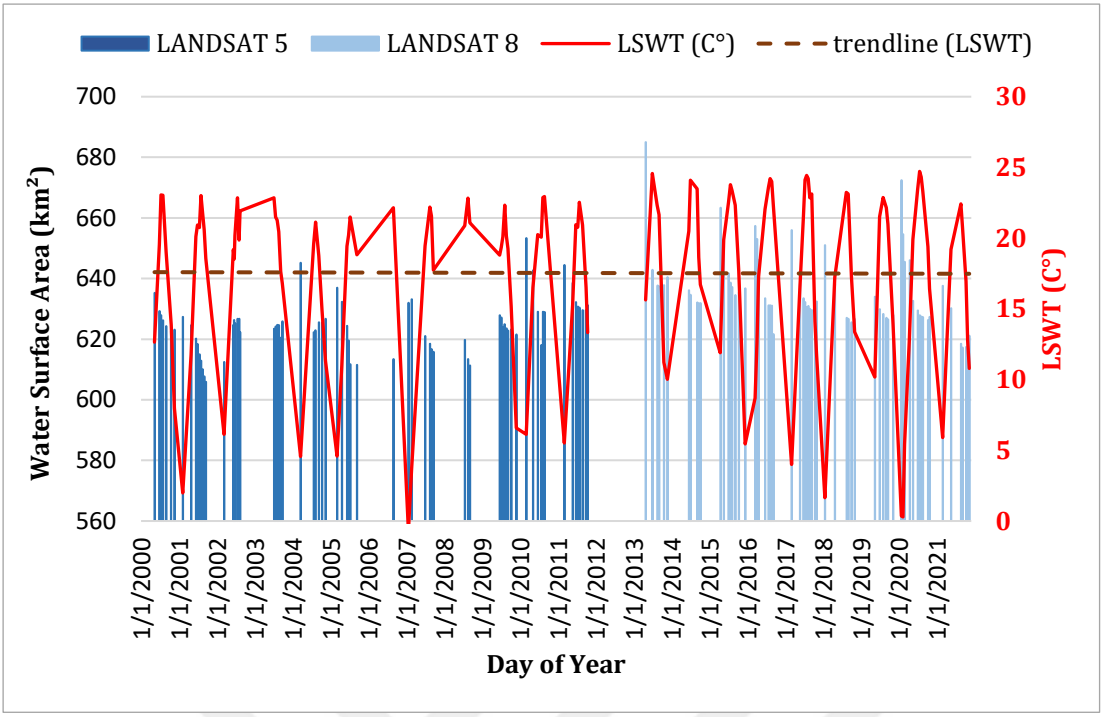

Figure 5.18 : The temporal changes in surface extent of Beysehir Lake with the LSWT variable.

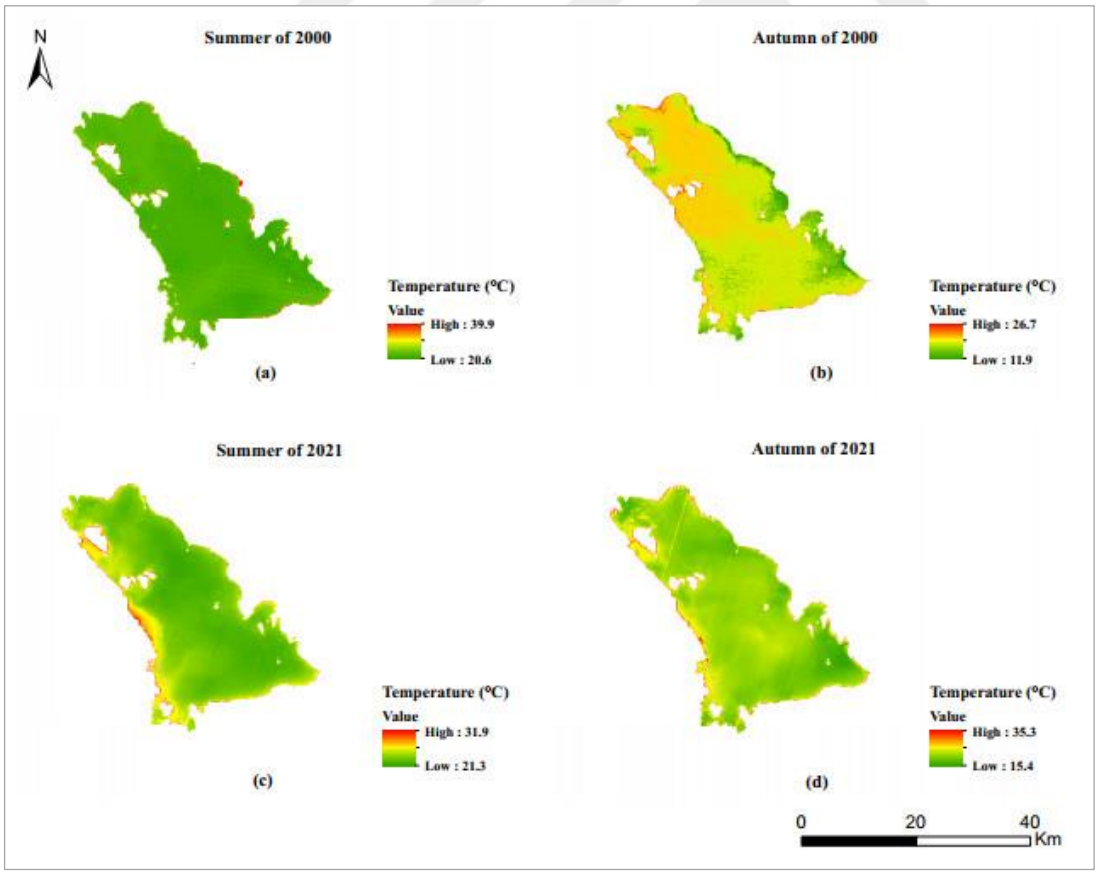

Figure 5.19 : The spatial changes of Beysehir Lake's surface area with LSWT for: (a) summer 2000, (b) autumn 2000, (c) summer 2021, and (d) autumn 2021.

Since there was no ground-based LST station in the region, we compared the average LSWT time series with MODIS LST for each lake. Figure 5.20 represents the scatter plot and correlation values between LSWT and MODIS LST for all three lakes. The correlation results were above 0.93 revealing that the obtained LSWT values are highly compatible with MODIS LST data (Albarqouni et al, 2022).

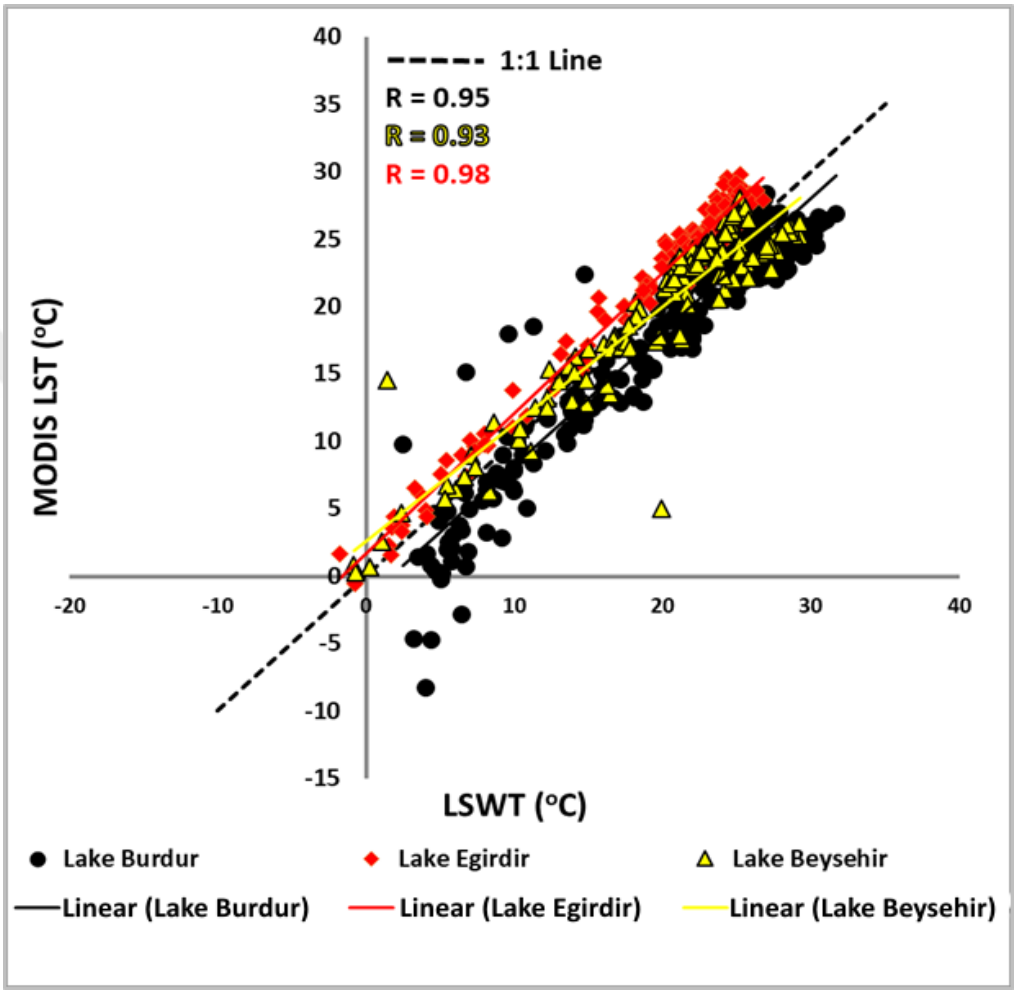

Figure 5.20 : Scatter plot and correlation values between LSWT and MODIS LST for all three lakes.

5.4 Meteorological Parameters and Correlation Analysis with LSWT and Lake Water Extent

To present meteorological effects on the obtained time series results, correlation analyses of LSWT and surface water area with meteorological parameters (temperature, precipitation and evaporation) were carried out. With this purpose, the correlation coefficient (R) was determined between LSWT and water surface area extent obtained from Landsat satellite images and meteorological parameters gathered

from ERA5-Land and TerraClimate datasets for each lake. ERA5-Land has available 50 variables and 4 parameters (temperature above 2 m, temperature of water surfaces (lake mix layer temperature), total evaporation and precipitation) were used in the study. TerraClimate dataset has 14 bands, whereas four bands, namely, total precipitation, evapotranspiration and temperature bands (minimum and maximum temperatures) were selected to use in the study. The average temperature was also calculated from minimum and maximum temperature bands.

With the aim of evaluating time series statistics of temperature datasets between the years 2000 and 2020, boxplots were created for each lake, which are shown in Figure 5.21. The boxplots are a summary of data distribution including maximum value, first quartile of data, median and mean values, third quartile of data and maximum value. Mean value is shown with 'x' in the box plots and the points above the maximum values (Figure 5.22a) are the outliers of data. Whereas LSWT and lake mix layer temperature are the surface temperature of the lake, temperature (2 m) of ERA5-Land and average temperature of TerraClimate are the air temperature. However, results show that LSWT and lake surface temperature data (lake mix layer temperature) cover the slightly same data range for all lakes in the period as it is expected.

While minimum, maximum and average LSWT values in Egirdir Lake show nearly close values to the lake mix layer temperature, the maximum values of lake mix layer temperature in Egirdir and Beysehir Lakes are higher than others. Additionally, lakes can be listed according to maximum temperature from largest to smallest as Burdur Lake, Beysehir Lake and Egirdir Lake, respectively. The main reason could be the geographic locations (elevation) of the lakes which are given in Table 3.1. According to that, Beysehir Lake is in the highest location among the lakes with 1124 m. Egirdir and Burdur Lakes are in 917 m and 857 m, respectively.

The other important parameters are precipitation and evaporation. According to statistics of these parameters for each lake (Figure 5.22), Burdur Lake has lower precipitation and higher evaporation than Egirdir Lake. Likewise, Egirdir Lake has lower precipitation and slightly higher evaporation than Beysehir Lake. However, the maximum precipitations of the lakes are quite different and Beysehir Lake has the highest precipitation value. It is found that precipitation and evapotranspiration statistics are also meaningful considering the water surface area results.

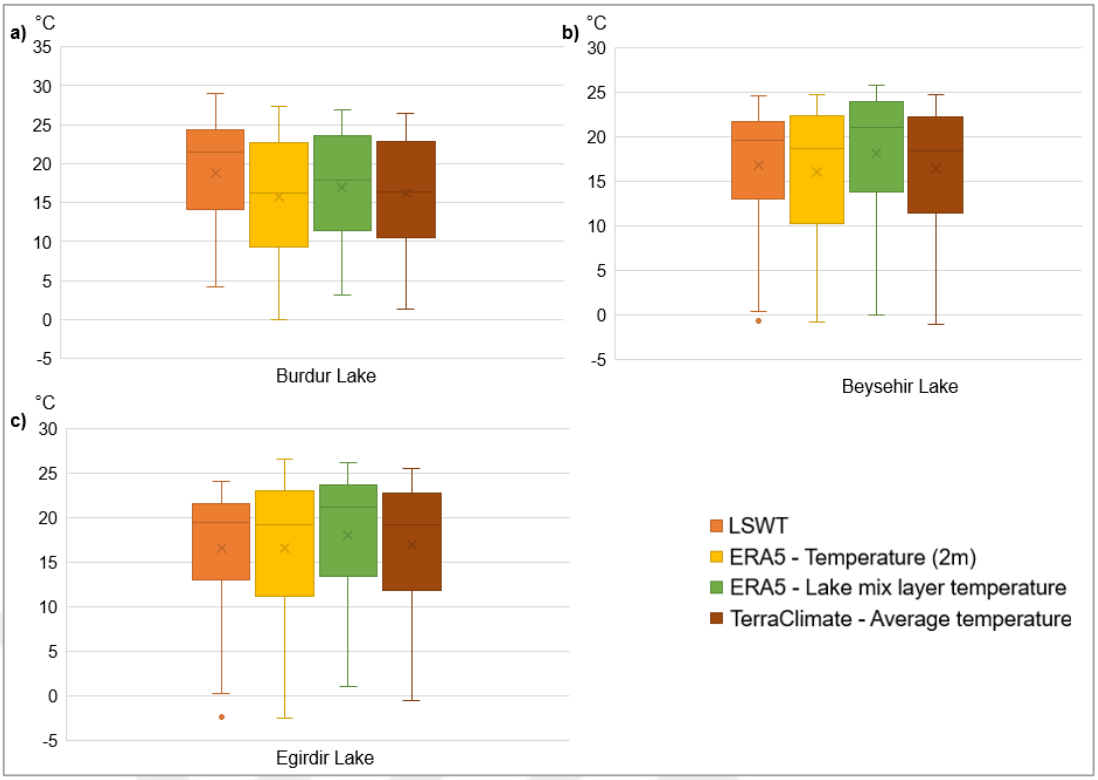

Figure 5.21 : Long term time series statistics of produced LSWT and temperature dataset of ERA5 and TerraClimate **(a)** Burdur Lake; **(b)** Beysehir Lake and **(c)** Egirdir Lake.

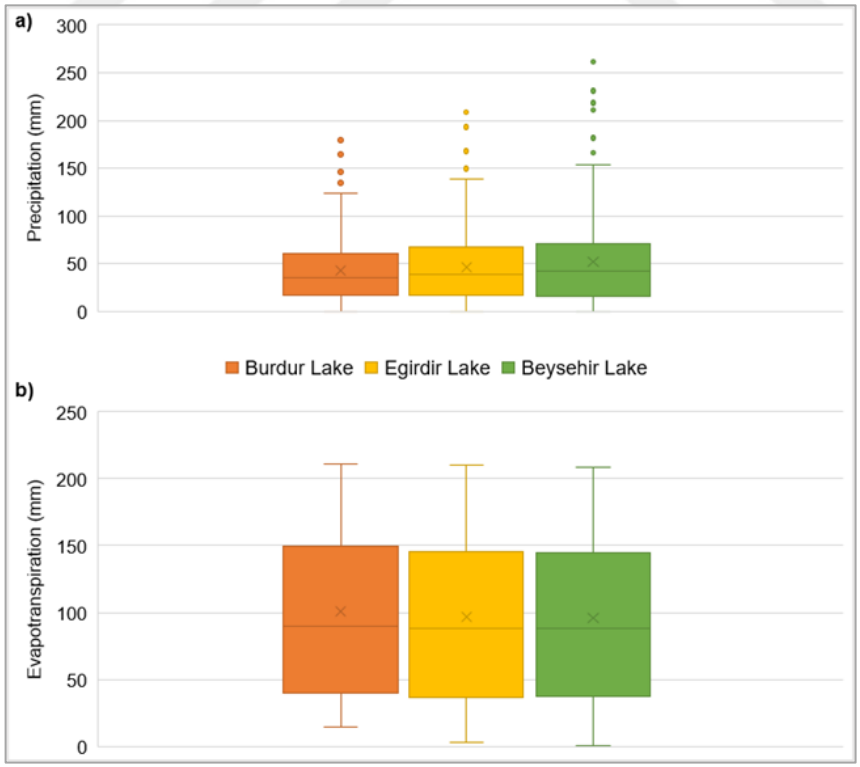

Figure 5.22 : Long term time series statistics of (a) precipitation and (b) evapotranspiration of TerraClimate for all lakes.

The monthly correlation analysis was performed with produced data (water surface area and LSWT) and climate parameters (temperature, precipitation and evaporation/evapotranspiration). Obtained R correlation coefficient values from correlation analysis are given in Table 5.3. R values were classified as: very high ($0.8 \leq R \leq 1.0$), high ($0.6 \leq R < 0.8$), moderate ($0.4 \leq R < 0.6$), low ($0.2 \leq R < 0.4$) and very low ($0 < R < 0.2$).

Besides, a 2-tailed statistical significance test was applied to reveal the degree of the relationship among the parameters. Statistical significance is often referred to as the p-value (probability value). The p value enables to figure out if there is a statistically significant correlation between two variables. As a general assumption, a $p<0.05$ shows statistical significance while $p<0.01$ is explained as high statistical significance. It was found that there is negative correlation between the LSWT and water surface area. The monthly correlation between water surface area and LSWT was found statistically highly significant ($p<0.01$) for all three lakes). However, the annual correlation was found statistically significant ($p<0.05$) for Egirdir Lake, and the annual correlation for Burdur and Beysehir Lakes was statistically insignificant ($p>0.05$). Because increasing air temperature and evaporation affected Burdur Lake's water surface area Firatli et al. (2022), and shrunk lake area has slightly increased the LSWT in time. One should also remember about the inertia of hydrological systems that have impact on the obtained correlation results.

Water surface area has also a statistically highly significant ($p<0.01$) monthly correlation with temperature and evaporation in Beysehir and Egirdir Lake, unlike Burdur Lake. Although it has the lowest precipitation and the highest temperature, there is no correlation between water surface area and all meteorological parameters of both datasets in Lake Burdur even though a 22% loss in water surface area. However, low and moderate correlations were determined on the annual scale.

TerraClimate average temperature shows statistically highly significant ($p<0.01$) correlation with LSWT for all lakes. The precipitation and temperature dataset in TerraClimate shows higher correlation than ERA-5 Land in Beysehir Lake. LSWT showed a statistically highly significant ($p<0.01$) correlation with evaporation and evapotranspiration values except for Beysehir lake, and the same pattern was observed for its correlation with precipitation in both datasets for all lakes. According to the results, it can be said that the sensitivity degree of Egirdir Lake to temperature and

evaporation is identical with Beysehir Lake. It could be related to the similar loss amount of water in these lakes. For all lakes, it is clear that the relationships between water surface area and other meteorological parameters are high for Beysehir Lake and Egirdir Lake, unlike Burdur Lake.

Table 5.3 : The monthly correlation analysis of meteorological parameters with LSWT and water surface area.

		Landsat	ERA5-Land				Terraclimate		
Lake	Monthly Correlation	LSWT	Temperature (2 m)	Lake mix layer temperature (°C)	Total evaporation (m)	Precipitation (mm)	Total Precipitation (mm)	Evapotranspiration (mm)	Average Temp
Burdur	Water surface area	0.207	0.008	0.01	0.066	0.063	0.061	0.095	0.028
	LSWT		0.507	0.478	0.567	0.224	0.194	0.576	0.524
Beysehir	Water surface area	0.418	0.595	0.576	0.517	0.495	0.432	0.317	0.46
	LSWT		0.806	0.858	0.929	0.349	0.651	0.857	0.944
Egirdir	Water surface area	0.768	0.61	0.613	0.447	0.388	0.346	0.564	0.716
	LSWT		0.964	0.972	0.872	0.599	0.53	0.872	0.96

very high	high	moderate	low	very low

6. CONCLUSIONS AND RECOMMENDATIONS

The primary purpose of this research is to use remote sensing images to examine the dynamic changes in surface water areas of Lake Burdur, Egirdir, and Beysehir in the Lakes Region, Türkiye during a 21-year period from 2000 to 2021. Additionally, the link between changes in water extent and lake surface water temperature (LSWT) was explored in order to get a better understanding of the causes of water extent change. Remote sensing analysis was carried out inside the GEE platform in order to facilitate the rapid and effective processing of a huge number of satellite imageries throughout this cloud environment. Analyses were done in this manner on the platform without the need to download images. Remote sensing images from the Landsat 5 TM and Landsat 8 OLI/TIRS collections were used to illustrate the research region. Between 2000 and 2021, a 10% cloud threshold was implemented to these images based on each lake borders.

The study includes a total of 606 images. Landsat 5 imagery was accessible from 2000 to 2011, whereas Landsat 8 imagery was available from 2013 until 2021, while there were no available images in 2012. To identify which pixels should be assessed as water, the NDWI was used; where NDWI greater than zero was considered as water. In the GEE Code Editor, NDWI values for all image collection were calculated using a function that employs the green and near-infrared bands. The results show that by using NDWI, water pixels can be extracted quite well, with an overall accuracy above 98% for each lake surface area. It has also been shown that the amount of lake surface area decreased has a direct correlation with the rise in LSWT values.

The following results are reached as a consequence of analyzing data during a 21-year period:

- Burdur Lake has lost almost 22% of its surface area while the LSWT has increased by more than 2.1° C, a reduction that began in 2000 and reached at 76.4% of its maximum extent in 2021.

- In Egirdir Lake, the surface water area did not drop below 94.8% of its maximum surface area. It had decreased slightly compared with the trend of decreasing for Burdur Lake, with less than 4% and increasing by more than 0.3° C in LSWT from 2000 to 2021.
- In Beysehir Lake, the water surface extent has decreased slightly by less than 1% during a 21-year period with a decrease of more than 1.4° C in LSWT. The surface lake decreased at the end of 2021 by 90.9% of its maximum surface area value

As shown in this study, remote sensing technologies and methodologies are necessary for monitoring lake surface areas and detecting their changes, and they should be properly employed by relevant institutions to ensure sustainable management.

Egirdir Lake is nearly three times larger than Burdur Lake and is farther from the city center than Burdur Lake. This circumstance may have resulted in Lake Egirdir being less impacted by human activity than Lake Burdur. In addition, the elevation of Egirdir Lake is higher than Burdur Lake, which affects the meteorological parameters. Thus, the rate of lake reduction may be affected by human activities, which may be taken into consideration in future studies.

Correlation analyses were realized for the water extent of each lake and LSWT with meteorological parameters of two different satellite datasets, namely ERA-5 Land and TerraClimate. Correlation results show that LSWT has a high correlation with air and surface temperature for all lakes and the water surface area of Beysehir and Egirdir lakes has moderate and high correlation with temperature datasets. Burdur Lake's water surface area has very low correlation with meteorological parameters which means that the shrinking of Burdur Lake is not directly related to the meteorological parameters. The common issues for water surface area changes were excessive water withdrawals and even the lakes themselves, primarily those of freshwater nature, lake usage for industrial reasons, and climate change effects.

All in all, the variations were more likely due to human-induced activities, especially for Lake Burdur. As a future perspective, all lake regions in Türkiye and further in the whole world can be analyzed with the same time series analysis to reveal their spatio-temporal changes. Besides, new datasets and methodologies may be compared to figure out the best solutions for this research design.

The sustainable usage concept must be used in order to protect lakes and to establish management plans for such regions. Thus, all conservation and exploitation operations throughout the concerned inland water areas should be organized by the management plan, which should serve as the basic regulation.

REFERENCES

Akher, S. K., & Chattopadhyay, S. (2017). Impact of Urbanization on Land Surface Temperature - A Case Study of Kolkata New Town. *The International Journal Of Engineering And Science (IJES)*, *6*(1), 71–81. https://doi.org/10.9790/1813-0601027181

Akşit, G. D. Semiz G. (2014). Water quality , surface area , evaporation and precipitation of Lake Burdur. *Food, Agriculture & Environment*, *11*(1), 751–753.

Albarqouni, M. M. Y., Yağmur, N., Bektaş Balçık, F., & Şekertekin, A. (2022). Assessment of Spatio-Temporal Changes in Water Surface Extents and Lake Surface Temperatures using Google Earth Engine for Lakes Region , Türkiye. *ISPRS International Journal of Geo-Information*, *11*(7), 407. https://doi.org/10.3390/ijgi1107040

Ali, M. I., Dirawan, G. D., Hasim, A. H., & Abidin, M. R. (2019). Detection of changes in surface water bodies urban area with NDWI and MNDWI methods. *International Journal on Advanced Science, Engineering and Information Technology*, *9*(3), 946–951. https://doi.org/10.18517/ijaseit.9.3.8692

Aslan, N., & Koc-San, D. (2021). Investigation of the changes of lake surface temperatures and areas: Case study of burdur and Egirdir Lakes, Turkey. *International Archives of the Photogrammetry, Remote Sensing and Spatial Information Sciences - ISPRS Archives*, *43*(B3-2021), 299–304. https://doi.org/10.5194/isprs-archives-XLIII-B3-2021-299-2021

Asokan, A., & Anitha, J. (2019). *Change detection techniques for remote sensing applications : a survey*. 143–160. https://doi.org/https://doi.org/10.1007/s12145-019-00380-5

Atalay, İ., & Efe, R. (2008). *Ecoregions of the Mediterranean Area and the Lakes Region of Turkey*. https://www.researchgate.net/publication/265181768_ecoregions_of_the_mediterranean_area_and_the_lakes_region_of_turkey

Avraz, A. D., Ener, E. Ş., Ener, Ş. Ş., & Varol, S. (2014). Water Balance of the Eğirdir Lake and the Influence of Budget Components, Isparta,Turkey. *Journal of Natural and Applied Science*, *18*(2), 27–36. https://dergipark.org.tr/en/pub/sdufenbed/issue/20804/222181

Bai, J., Chen, X., Li, J., Yang, L., & Fang, H. (2011). *Changes in the area of inland lakes in arid regions of central Asia during the past 30 years*. 247–256. https://doi.org/10.1007/s10661-010-1686-y

Behera, M. D., Chitale, V. S., Shaw, A., Roy, P. S., & Murthy, M. S. R. (2012). Wetland Monitoring, Serving as an Index of Land Use Change-A Study in Samaspur Wetlands, Uttar Pradesh, India. *Journal of the Indian Society of Remote Sensing*, *40*(2), 287–297. https://doi.org/10.1007/s12524-011-0139-6

Bostan, H. (2017). Social Structural Changes, Related Problems and Proposed Solutions Caused By Internal Migrations in Turkey. *Journal of Geography*, *35*, 1–16. https://doi.org/10.26650/JGEOG330955

Buma, W. G., Lee, S. Il, & Seo, J. Y. (2018). Recent surface water extent of lake Chad from multispectral sensors and GRACE. *Sensors (Switzerland)*, *18*(7). https://doi.org/10.3390/s18072082

Cevik, M. (2009). *Lake Beysehir*. National Nature and Culture Documentaries Association. https://dogabel.wordpress.com/

Ceyhan, E. (2016). *Multi-Temporal Water Extent Analysis of A Hypersaline Playa Lake Using Landsat Imagery*, Ms.c Thesis. Institute of Science and Technology ODTU, Ankara, Turkey, Available online: https://open.metu.edu.tr/handle/11511/25749 (accessed on 06 April 2022).

Chang H., Chen Y., Zhang S., & J. W. (2018). Reviews of Geophysics Detecting , Extracting , and Monitoring Surface Water From Space Using Optical Sensors : A Review. *AGU*, *56*, 333–360. https://doi.org/10.1029/2018RG000598

Chen, B., Chen, L., Huang, B., Michishita, R., & Xu, B. (2018). ISPRS journal of photogrammetry and Remote Sensing dynamic monitoring of the Poyang Lake wetland by integrating Landsat and MODIS observations. *ISPRS Journal of Photogrammetry and Remote Sensing*, *139*, 75–87. https://doi.org/10.1016/j.isprsjprs.2018.02.021

Dai, A. (2013). Increasing drought under global warming in observations and models. *Nature Climate Change*, *3*(1), 52–58. https://doi.org/10.1038/nclimate1633

Dervisoglu, A. (2021). Analysis of the temporal changes of inland ramsar sites in turkey using google earth engine. *ISPRS International Journal of Geo-Information*, *10*(8). https://doi.org/10.3390/ijgi10080521

Dörnhöfer, K., & Oppelt, N. (2016). Remote sensing for lake research and monitoring - Recent advances. *Ecological Indicators*, *64*, 105–122. https://doi.org/10.1016/j.ecolind.2015.12.009

Du, Y., Zhang, Y., Ling, F., Wang, Q., Li, W., & Li, X. (2016). Water bodies' mapping from Sentinel-2 imagery with Modified Normalized Difference Water Index at 10-m spatial resolution produced by sharpening the swir band. *Remote Sensing*, *8*(4). https://doi.org/10.3390/rs8040354

Du, Z., Linghu, B., Ling, F., Li, W., Tian, W., Wang, H., Gui, Y., Sun, B., & Zhang, X. (2012). Estimating surface water area changes using time-series Landsat data in the Qingjiang River Basin, China. *Journal of Applied Remote Sensing*, *6*(1), 063609. https://doi.org/10.1117/1.jrs.6.063609

Feng, L., Hou, X., & Zheng, Y. (2019). Monitoring and understanding the water transparency changes of fifty large lakes on the Yangtze Plain based on long-term MODIS observations. *Remote Sensing of Environment*, *221*(November 2018), 675–686. https://doi.org/10.1016/j.rse.2018.12.007

Fethi, Ileri, A. & K. (2015). Eğirdir ve Beyşehir göllerinin uydu verileri ve topoğrafik harita yardımıyla kıyı çizgisi değişimleri. *Doğal Kaynaklar ve Ekonomi Bülteni 20*, 37–45. (In Turkish)

Feyisa, G. L., Meilby, H., Fensholt, R., & Proud, S. R. (2014). Remote Sensing of Environment Automated Water Extraction Index : A new technique for surface water mapping using Landsat imagery. *Remote Sensing of Environment*, *140*, 23–35. https://doi.org/10.1016/j.rse.2013.08.029

Firatli, E., Dervisoglu, A., Yagmur, N., Musaoglu, N., & Tanik, A. (2022). Spatio-temporal assessment of natural lakes in Turkey. *Earth Science Informatics*. https://doi.org/10.1007/s12145-022-00778-8

***General Directorate of Water Management*.** (2015). General Directorate of Water Management. Available online: https://www.tarimorman.gov.tr/SYGM/Sayfalar/EN/AnaSayfa.aspx. (accessed on 05 April 2022)

Gorelick, N., Hancher, M., Dixon, M., Ilyushchenko, S., Thau, D., & Moore, R. (2017). Remote Sensing of Environment Google Earth Engine : Planetary-scale geospatial analysis for everyone. *Remote Sensing of Environment*, *202*, 18–27. https://doi.org/10.1016/j.rse.2017.06.031

Gorguner, M., & Kavvas, M. L. (2020). Science of the Total Environment Modeling impacts of future climate change on reservoir storages and irrigation water demands in a Mediterranean basin. *Science of the Total Environment*, *748*, 141246. https://doi.org/10.1016/j.scitotenv.2020.141246

Gözükara, G., Altunbaş, S., & Sarı, M. (2019). Burdur Gölü'ndeki seviye değişimi sonucunda ortaya çıkan lakustrin materyalin zamansal ve mekansal değişimi. *Anadolu Journal Of Agricultural Sciences*, *34*(3), 386–396. https://doi.org/10.7161/omuanajas.556215. (In Turkish)

Harvey, K. R., & Hill, G. J. E. (2010). *Vegetation mapping of a tropical freshwater swamp in the Northern Territory , Australia : A comparison of aerial photography , Landsat TM and SPOT satellite imagery*. *1161*, 2911–2925. https://doi.org/10.1080/01431160119174

Hird, J. N., Delancey, E. R., & Mcdermid, G. J. (2017). Google earth engine, open-access satellite data, and machine learning in support of large-area probabilistic wetland mapping. *Remote Sensing*, 9 (12), 1315. https://doi.org/10.3390/rs9121315

Holben, B. N. (1986). Characteristics of maximum-value composite images from temporal AVHRR data. *International Journal of Remote Sensing*, *7*(11), 1417–1434. https://doi.org/10.1080/01431168608948945

Huang, C., Chen, Y., Zhang, S., & Wu, J. (2018). Detecting, Extracting, and Monitoring Surface Water From Space Using Optical Sensors: A Review. *Reviews of Geophysics*, *56*(2), 333–360. https://doi.org/10.1029/2018RG000598

Ji, L., Geng, X., Sun, K., Zhao, Y., & Gong, P. (2015). Target detection method for water mapping using landsat 8 OLI/TIRS Imagery. *Water (Switzerland)*, *7*(2), 794–817. https://doi.org/10.3390/w7020794

Jiang, H., Feng, M., Zhu, Y., Lu, N., Huang, J., & Xiao, T. (2014). An automated method for extracting rivers and lakes from Landsat imagery. *Remote Sensing*, *6*(6), 5067–5089. https://doi.org/10.3390/rs6065067

K.M., A. S., Almotairi, K. H., Alswaitti, M., Amr, S. S. A., Alkarkhi, A. F. M., Taşoğlu, E., & Hussein, A. M. (2021). Effects of meteorological parameters on surface water loss in burdur lake, turkey over 34 years landsat google earth engine time-series. *Land*, *10*(12). https://doi.org/10.3390/land10121301

Kale, S., & Acarlı, D. (2019). Spatial and Temporal Change Monitoring in Water Surface Area of Atikhisar Reservoir (Çanakkale, Turkey) by using Remote Sensing and Geographic Information System Techniques. *Alınteri Zirai Bilimler Dergisi*, *34*, 47–56. https://doi.org/10.28955/alinterizbd.574361

Li, S., Sun, D., Goldberg, M. D., Sjoberg, B., Santek, D., Ho, J. P., Deweese, M., Restrepo, P., Lindsey, S., & Holloway, E. (2018). *Remote Sensing of Environment Automatic near real-time fl ood detection using Suomi-NPP / VIIRS data*. *204*(September 2017), 672–689. https://doi.org/10.1016/j.rse.2017.09.032

Li, S., Sun, D., Goldberg, M., & Stefanidis, A. (2013). Derivation of 30-m-resolution water maps from TERRA/MODIS and SRTM. *Remote Sensing of Environment*, *134*, 417–430. https://doi.org/10.1016/j.rse.2013.03.015

Li, W., Du, Z., Ling, F., Zhou, D., Wang, H., Gui, Y., Sun, B., & Zhang, X. (2013). A comparison of land surface water mapping using the normalized difference water index from TM, ETM+ and ALI. *Remote Sensing*, *5*(11), 5530–5549. https://doi.org/10.3390/rs5115530

Masocha, M., Dube, T., Makore, M., Shekede, M. D., & Funani, J. (2018). Surface water bodies mapping in Zimbabwe using landsat 8 OLI multispectral imagery: A comparison of multiple water indices. *Physics and Chemistry of the Earth*, 106, 63–67. https://doi.org/10.1016/j.pce.2018.05.005

McFeeters, S. K. (1996). The use of the Normalized Difference Water Index (NDWI) in the delineation of open water features. *International Journal of Remote Sensing*, *17*(7), 1425–1432. https://doi.org/10.1080/01431169608948714

McHugh, M. L. (2012). Lessons in biostatistics interrater reliability : the kappa statistic. *Biochemica Medica*, *22*(3), 276–282. https://www.biochemia-medica.com/en/journal/22/3/10.11613/BM.2012.031

Messager, M. L., Lehner, B., Grill, G., Nedeva, I., & Schmitt, O. (2016). Estimating the volume and age of water stored in global lakes using a geo-statistical approach. *Nature Communications*, *7*, 1–11. https://doi.org/10.1038/ncomms13603

Mueller, N., Lewis, A., Roberts, D., Ring, S., Melrose, R., Sixsmith, J., Lymburner, L., Mcintyre, A., Tan, P., Curnow, S., & Ip, A. (2016). *Remote Sensing of Environment Water observations from space : Mapping surface water from 25 years of Landsat imagery across Australia*. *174*, 341–352. https://doi.org/10.1016/j.rse.2015.11.003

Ndossi, M. I., & Avdan, U. (2016). Application of open source coding technologies in the production of Land Surface Temperature (LST) maps from Landsat: A PyQGIS plugin. *Remote Sensing*, *8*(5). https://doi.org/10.3390/rs8050413

O'Reilly, C. M., Rowley, R. J., Schneider, P., Lenters, J. D., Mcintyre, P. B., & Kraemer, B. M. (2015). Rapid and highly variable warming of lake surface waters around the globe. *Geophysical Research Letters*, 42, 1-9. https://doi.org/10.1002/2015GL066235

Ouma, Y. O., & Tateishi, R. (2007). Lake water body mapping with multiresolution based image analysis from medium-resolution satellite imagery. *International Journal of Environmental Studies*, *64*(3), 357–379. https://doi.org/10.1080/00207230500196856

Ozesmi, S. L., & Bauer, M. E. (2002). Satellite remote sensing of wetlands. *Wetlands Ecology and Management*, *10*(5), 381–402. https://doi.org/10.1023/A:1020908432489

Ramsar. (2006). Wetlands: a global disappearing act, (78). Available online: https://slidelegend.com/wetlands-a-global-disappearing-act-ramsar_59d42edf1723ddcbff06fd1d.html. (accessed on 06 April 2022).

Rokni, K., Ahmad, A., Selamat, A., & Hazini, S. (2014). Water Feature Extraction and Change Detection Using Multitemporal Landsat Imagery. *Remote Sensing*, *5*(6), 4173–4189. https://doi.org/10.3390/rs6054173

Sarp, G., & Ozcelik, M. (2017). Water body extraction and change detection using time series: A case study of Lake Burdur, Turkey. *Journal of Taibah University for Science*, *11*(3), 381–391. https://doi.org/10.1016/j.jtusci.2016.04.005

Sisay, A. (2016). Remote Sensing Based Water Surface Extraction and Change Detection in the Central Rift Valley Region of Ethiopia. *American Journal of Geographic Information System*, *5*(2), 33–39. https://doi.org/10.5923/j.ajgis.20160502.01

Sobrino, J. A.; Jiménez-Muñoz, J. C.; Paolini, L. (2004). Land surface temperature retrieval from LANDSAT TM 5. *Remote Sensing of Environment*, *90*(4), 434–440. https://doi.org/10.1016/j.rse.2004.02.003

Soltani, K., Amiri, A., Zeynoddin, M., Ebtehaj, I., Gharabaghi, B., & Bonakdari, H. (2021). Forecasting monthly fluctuations of lake surface areas using remote sensing techniques and novel machine learning methods. *Theoretical and Applied Climatology*, *143*(1–2), 713–735. https://doi.org/10.1007/s00704-020-03419-6

Stehman, S. V. (2014). Estimating area and map accuracy for stratified random sampling when the strata are different from the map classes. *International Journal of Remote Sensing*, *35*(13), 4923–4939. https://doi.org/10.1080/01431161.2014.930207

Thomas L., Ralph W., Kiefer, J. C. (2008). *Remote Sensing and Image Interpretation (Fifth Edition). The Geographical Journal*. New Jersey, *146*(3), 448–449.

Turkish State Meteorological Service. (2021). *Areal Precipitation Report*. Available online: https://www.mgm.gov.tr/veridegerlendirme/yagis-raporu.aspx (accessed on 5 May 2022).

U.S. Geological Survey. (2019). Using the USGS Landsat Level-1 Data Product. In *United States Geological Survey* (pp. 3–5). Available online: https://www.usgs.gov/landsat-missions/using-usgs-landsat-level-1-data-product (accessed on 06 April 2022)

Valor, E. (1996). Mapping land surface emissivity from NDVI: Application to European, African, and South American 773 areas. *Remote Sensing of Environment*, *57*, 167–184. https://doi.org/https://doi.org/10.1016/0034-4257(96)00039-9

Wang, R., Xia, H., Qin, Y., Niu, W., Pan, L., Li, R., Zhao, X., Bian, X., & Fu, P. (2020). Dynamic monitoring of surface water area during 1989–2019 in the hetao plain using landsat data in google earth engine. *Water (Switzerland)*, *12*(11), 1–21. https://doi.org/10.3390/w12113010

Wang, X., Xiao, X., Zou, Z., Chen, B., Ma, J., Dong, J., Doughty, R. B., Zhong, Q., Qin, Y., Dai, S., Li, X., Zhao, B., & Li, B. (2020). Tracking annual changes of coastal tidal flats in China during 1986–2016 through analyses of Landsat images with Google Earth Engine. *Remote Sensing of Environment*, *238* (November 2018). https://doi.org/10.1016/j.rse.2018.11.030

Wang, Y., Ma, J., Xiao, X., Wang, X., Dai, S., & Zhao, B. (2019). Long-term dynamic of Poyang Lake surface water: A mapping work based on the Google Earth Engine cloud platform. *Remote Sensing*, *11*(3). https://doi.org/10.3390/rs11030313

Wendleder, A., Friedl, P., & Mayer, C. (2018). Impacts of climate and supraglacial lakes on the surface velocity of Baltoro Glacier from 1992 to 2017. *Remote Sensing*, *10*(11), 1–25. https://doi.org/10.3390/rs10111681

Weng, Q., Lu, D., & Schubring, J. (2004). Estimation of land surface temperature-vegetation abundance relationship for urban heat island studies. *Remote Sensing of Environment*, *89*(4), 467–483. https://doi.org/10.1016/j.rse.2003.11.005

***WWF*.** (2008). Ramsar sites evaluation report in Turkey. In *WWF*. Available online: http://awsassets.wwftr.panda.org/downloads/wwf_turkiye_ramsar_alanlari_degerlendirme_raporu.pdf. (accessed on 06 Abril 2022)

Xia, H., Zhao, J., Qin, Y., Yang, J., Cui, Y., Song, H., Ma, L., Jin, N., & Meng, Q. (2019). Changes in water surface area during 1989-2017 in the Huai River Basin using Landsat data and Google earth engine. *Remote Sensing*, *11*(15). https://doi.org/10.3390/rs11151824

Xie, C., Zhang, X., Zhuang, L., Zhu, R., & Guo, J. (2022). Analysis of surface temperature variation of lakes in China using MODIS land surface temperature data. *Scientific Reports*, 1–13. https://doi.org/10.1038/s41598-022-06363-9

Xu, H. (2007). Modification of normalised difference water index (NDWI) to enhance open water features in remotely sensed imagery. *International Journal of Remote Sensing*, *14*(27), 3025-3033. https://doi.org/10.1080/01431160600589179

Yagmur, N., Bilgilioglu, B. B., Musaoglu, N., & Erten, E. (2018). Temporal Changes of Lentic System Surfaces in Konya Closed Basin , Turkey. *International Journal of Remote Sensing*, *1*(10), 2891-2896. https://www.researchgate.net/publication/325334702_Temporal_Changes_of_Lentic_System_Surfaces_in_Konya_Closed_Basin_Turkey

Yang, X., Zhao, S., Qin, X., Zhao, N., & Liang, L. (2017). Mapping of Urban Surface Water Bodies from Sentinel-2 MSI Imagery at 10 m Resolution via NDWI-Based Image Sharpening. *Remote Sensing*, *9*(6), 1–19. https://doi.org/10.3390/rs9060596

Zhang, F., Tiyip, T., Kung, H. te, Johnson, V. C., Wang, J., & Nurmemet, I. (2016). Improved water extraction using Landsat TM/ETM+ images in Ebinur Lake, Xinjiang, China. *Remote Sensing Applications: Society and Environment*, *4*, 109–118. https://doi.org/10.1016/j.rsase.2016.08.001

Zhou, Y., Dong, J., Xiao, X., Xiao, T., Yang, Z., Zhao, G., Zou, Z., & Qin, Y. (2017). Open surface water mapping algorithms: A comparison of water-related spectral indices and sensors. *Water (Switzerland)*, *9*(4). https://doi.org/10.3390/w9040256

URL-1. EPA, <https://19january2017snapshot.epa.gov/climate-impacts/climate-impacts-water-resources_.html>, data retrieved 06 May 2022.

URL-2. USGS. <https://www.usgs.gov/faqs/what-remote-sensing-and-what-it-used#:~:text=Remote sensing is the process,sense%22 things about the Earth>, data retrieved 06 April 2022.

URL-3. Burdur Governor of the Republic of Turkey; Burdur Governor of the Republic of Turkey, < http://www.burdur.gov.tr/>, data retrieved 06 April 2022.

URL-4. Ministry of Agriculture and Forestry (MoAF), General Directorate of Nature Conservation and National Parks. <https://saybis.tarimorman.gov.tr/#>, data retrieved 06 April 2022.

URL-5. NASA, <https://landsat.gsfc.nasa.gov/about/technical-information/>, data retrieved 07 April 2022.

URL-6. USGS. <https://www.usgs.gov/faqs/what-are-band-designations-landsat-satellites#:~:text=Thermal bands 10 and 11,106 mi by 114 mi >, data retrieved 05 April 2022.

URL-7. ERA5 Land, <https://cds.climate.copernicus.eu/cdsapp#!/dataset/reanalysis-era5-land-monthly-means?tab=overview>, data retrieved 07 May 2022.

URL-8. TerraClimate. <https://www.climatologylab.org/terraclimate.html>, data retrieved 06 May 2022

URL-9. Google Earth Engine, <https://developers.google.com/earth-engine/datasets>, data retrieved 07 April 2022.

CURRICULUM VITAE

Name Surname : Mohammed M. Y. Albarqouni

EDUCATION

- **B.Sc.** **:** 2018, The Islamic University of Gaza, Civil Engineering Faculty, Civil Engineering Department

PUBLISHED ARTICLE

- **Albarqouni, M. M. Y., Yağmur, N., Bektaş Balçık, F., & Şekertekin, A.** (2022). Assessment of Spatio-Temporal Changes in Water Surface Extents and Lake Surface Temperatures using Google Earth Engine for Lakes Region, Türkiye. *ISPRS International Journal of Geo Information*, *11*(7), 407.